Published in final edited form as:
Dev Dyn. 2009 March ; 238(3): 532–553. doi:10.1002/dvdy.21862.

The Allantoic Core Domain: New Insights Into Development of the Murine Allantois and Its Relation to the Primitive Streak

Karen M. Downs[1,*], **Kimberly E. Inman**[1], **Dexter X. Jin**[1], and **Allen C. Enders**[2]

[1]Department of Anatomy, University of Wisconsin-Madison School of Medicine and Public Health, Madison, Wisconsin

[2]Department of Cell Biology and Human Anatomy, Room 3301 Tupper Hall, University of California-Davis, Davis, California

Abstract

The whereabouts and properties of the posterior end of the primitive streak have not been identified in any species. In the mouse, the streak's posterior terminus is assumed to be confined to the embryonic compartment, and to give rise to the allantois, which links the embryo to its mother during pregnancy. In this study, we have refined our understanding of the biology of the murine posterior primitive streak and its relation to the allantois. Through a combination of immunostaining and morphology, we demonstrate that the primitive streak spans the posterior extraembryonic and embryonic regions at the onset of the neural plate stage (~7.0 days postcoitum, dpc). Several hours later, the allantoic bud emerges from the extraembryonic component of the primitive streak (XPS). Then, possibly in collaboration with overlying allantois-associated extraembryonic visceral endoderm, the XPS establishes a germinal center within the allantois, named here the Allantoic Core Domain (ACD). Microsurgical removal of the ACD beyond headfold (HF) stages resulted in the formation of allantoic regenerates that lacked the ACD and failed to elongate; nevertheless, vasculogenesis and vascular patterning proceeded. In situ and transplantation fate mapping demonstrated that, from HF stages onward, the ACD's progenitor pool contributed to the allantois exclusive of the proximal flanks. By contrast, the posterior intraembryonic primitive streak (IPS) provided the flanks. Grafting the ACD into T^C/T^C hosts, whose allantoises are significantly foreshortened, restored allantoic elongation. These results revealed that the ACD is essential for allantoic elongation, but the cues required for vascularization lie outside of it. On the basis of these and previous findings, we conclude that the posterior primitive streak of the mouse conceptus is far more complex than was previously believed. Our results provide new directives for addressing the origin and development of the umbilical cord, and establish a novel paradigm for investigating the fetal/placental relationship.

Keywords

ACD; allantois; Brachyury; chorio-allantoic fusion; elongation; mouse; niche; Oct-3/4; placentation; primitive streak; stem cells; T; umbilical cord; vascularization; visceral endoderm

[*]Correspondence to: Karen M. Downs, Department of Anatomy, University of Wisconsin-Madison School of Medicine and Public Health, 1300 University Avenue, Madison, WI 53706. kdowns@wisc.edu .

INTRODUCTION

The conceptus of eutherian mammals is composed of intimately juxtaposed embryonic and extraembryonic tissues. Principal among the latter is the chorio-allantoic placenta, which is created by fusion between the chorion and the allantois, two organ anlagen initially physically well separated within the exocoelomic cavity. Results of morphological studies (Sobotta, 1911) led to the current view that the allantois originates within the posterior primitive streak, whose caudal limit is confined to the embryo proper. Fate mapping further supported this view, demonstrating that proximal epiblast is converted into mesoderm within the posterior primitive streak, some of which is displaced into the allantois (Copp et al., 1986; Tam and Beddington, 1987; Lawson et al., 1991; Kinder et al., 1999). The allantois is then assumed to elongate as a result of sustained activity of the posterior intraembryonic primitive streak (hereafter referred to as the "IPS"). Ultimately, the allantois grows far enough through the exocoelom to fuse with the chorion to create the chorio-allantoic placenta.

Early localization studies of Brachyury (T), the founding member of the T-box family of transcription factors (Papaioannou, 2001), supported Sobotta's assumption that the primitive streak's rostral and caudal extremities are limited to the embryo proper. The allantois and embryonic anteroposterior (A–P) axis, the primitive streak, are both foreshortened in homozygous *T*/*T* embryos (Dobrovolskaia-Zavadskaia, 1927; Gluecksohn-Schoenheimer, 1944). T was identified in the embryonic primitive streak at all stages examined, but only occasionally in the allantois (Wilkinson et al., 1990; Herrmann, 1991). Consequently, these observations suggested that the *T*/*T* allantoic defect is secondary to a primary one in the IPS (Naiche et al., 2005). Furthermore, they perpetuated Sobotta's claim that the primitive streak is limited to the embryo proper, a conclusion that has made its way into a large number of original studies (e.g., Crossley and Martin, 1995), reviews (e.g., Tam and Beddington, 1992; Beddington and Robertson, 1999), and textbooks (e.g., Wolpert et al., 1998).

Recent evaluation of the allantois over developmental intervals separated by 2–4 hr, rather than the widely spaced intervals used in the collective studies, above, revealed that the allantois uninterruptedly exhibits T-positive cells. These localized to its proximal core from the late bud (LB; ~7.5 days post coitum [dpc]) through 5-somite pair (−s) (~8.5 dpc) stages (Inman and Downs, 2006a). Subsequent investigation into the role of T through study of $T^{Curtailed}$ homozygous mutants (T^C/T^C) demonstrated an intrinsic role for T in allantoic development (Inman and Downs, 2006b). The mitotic index was significantly reduced in T^C/T^C allantoises, and corresponded to a reduction in allantoic cell number, contributing to foreshortening of the allantoic projection. In addition, the T^C/T^C allantoic core died, leaving behind a short allantoic remnant. Although T^C/T^C allantoic remnants appropriately expressed Vascular Cell Adhesion Molecule-1 (VCAM-1), a molecular component of chorio-allantoic fusion (Gurtner et al., 1995; Kwee et al., 1995), T^C/T^C allantoises invariably failed to elongate far enough to fuse with the chorion. By contrast, the IPS of T^C/T^C mutants exhibited no diminution in mitotic index during the period of allantoic failure. In fact, cell movement from the mutant T^C/T^C IPS contributed to the T^C/T^C allantois, and the T^C/T^C IPS exhibited little-to-no cell death. Together, localization and cellular behavior demonstrated that T plays an intrinsic role in allantoic development; the IPS is not a priori responsible for the defects observed in T^C/T^C mutant allantoises.

In this study, we investigated the origin and nature of the T-defined allantoic core and, especially, its relationship to Sobotta's "classically" defined IPS, from just before the appearance of the allantoic bud (~7.0 dpc) through chorioallantoic fusion (~8.5 dpc), a period that encompasses thirteen developmental time points during which the allantois elongates (Downs and Bertler, 2000) and vascularizes (Downs et al., 1998). Unexpectedly, we discovered that, just before the allantoic bud appeared, the primitive streak extended into the

extraembryonic region. Then, over the next 4–8 hr, the allantoic bud emerged from this extraembryonic posterior primitive streak (XPS). Through interaction with the overlying allantois-associated extraembryonic visceral endoderm (AX), the XPS expanded into a germinal center, which we call the Allantoic Core Domain (ACD). The properties of the ACD were distinct from those of the IPS; in particular, the ACD supplied the bulk of cells to the allantois and was essential for allantoic elongation to the chorion, while the IPS supplied cells only to its proximal flanks. Together, the two posterior regions of the primitive streak, the XPS and IPS, establish the nascent umbilical cord. These results reveal that the posterior end of the primitive streak is not limited to the embryo proper and that its relationship to the allantois is far more complex than has been appreciated.

RESULTS

The Primitive Streak Extends Into the Posterior Extraembryonic Region

Given that diverse tissue preparations can affect the outcome of immunostaining for the same protein (Downs et al., 2002; Inman and Downs, 2006a; Downs, 2008), we reinvestigated the whereabouts of T in the primitive streak and allantois. A whole-mount immunostaining technique superior to standard fixation and sectional analysis (Downs, 2008) was applied to conceptuses at finely spaced developmental intervals, separated by 2–4 hr. In particular, the "No Bud" (OB) stage, which is equivalent to the onset of the neural plate stage just before the appearance of the allantois (Downs and Davies, 1993), was included here. This stage had not been examined in previous studies (Inman and Downs, 2006a).

At all stages, T-positive cells were found in all hitherto documented cell types, including embryonic epiblast, nascent mesoderm, the embryonic primitive streak and its anterior derivatives, the node and notochord, as well as in unrelated cell lineages, including chorionic ectoderm and extraembryonic visceral endoderm, where T localized to the cytoplasm rather than the nucleus (Fig. 1, and data not shown; Inman and Downs, 2006a). Intriguingly, at the OB-LB stages, the T-positive posterior primitive streak, which localizes to and defines the midline of the embryo, extended into the extraembryonic region where it was closely juxtaposed to overlying visceral endoderm (Fig. 1A–F). From this presumptive XPS, the allantoic bud emerged (Fig. 1E); a few round T-positive cells were observed in the bud's distal region (Fig. 1E), but those of the proximal allantoic XPS were flat, and intimately associated with overlying visceral endoderm, referred to hereafter as the "allantois-associated extraembryonic visceral endoderm," or AX. The T-positive XPS reached a distance of ~150 micrometers (μm), or approximately 15 nuclear diameters, from the amniotic/embryonic border. At the LB stage, the proximal portion of the XPS had thickened, while its more distal region was enlarging; many round T-positive cells were conspicuous throughout the projection (Fig. 1F).

Thus, T immunostaining suggested the compelling possibility that the posterior end of the primitive streak is not limited to the embryo proper, but extends into the extraembryonic region where, a few hours later, it gives rise to the allantoic bud. Careful morphological analysis in plastic and transmission electron microscopy (TEM) supported this view, revealing that, at the OB stage, the primitive streak's posterior limit was located within the extraembryonic region as a dense wedge of cells closely juxtaposed to the overlying visceral endoderm. Its cells were both continuous with and morphologically similar to those of the intraembryonic primitive streak (IPS; Fig. 2A,B). A few hours later, the streak's extraembryonic limit exhibited deeply azurephilic elongated cells which formed a column several cells deep and bore the same intensity of staining and polarity as those in the IPS (Fig. 2C). Ultrastructural analyses confirmed continuity between the extraembryonic and intraembryonic regions of the primitive streak (Fig. 2G,H; and data not shown). Cells of both streak compartments were tightly packed, and exhibited only an occasional intercellular adhesion junction and few filopodia (not shown).

By the very early headfold (vEHF) stage, the polarized rows of T-positive cells were disappearing from contact with the AX, replaced by round ones that expanded into the core of the allantois (Fig. 1G,H). Plastic and TEM sectional analysis confirmed that the deeply azurephilic polarized files of cells had expanded into the core of the allantois (Fig. 2D) and persisted there through 5-s (Fig. 2E,F, and data not shown), when our plastic analysis ended. Cellular associations became further apart (Fig. 2I), and contact was retained between them by simple adhesion junctions (Fig. 2J). At all stages, the proximal core cells appeared relatively undifferentiated, characterized by abundant free polyribosomes, large irregularly indented nuclei with conspicuous nucleoli, and a spherical Golgi region, but only a few strands of rough endoplasmic reticulum and some scattered mitochondria. These properties accorded with the presence of abundant Oct-3/4 protein, characteristic of undifferentiated and germ cells (Scholer, 1991) in the base of the allantois (Downs, 2008).

Transverse sections through the allantois (EHF-6-s) revealed that both T-and Oct-3/4–positive cells constituted an overlapping domain centered on the A–P axis but which was asymmetric about the dorsoventral (D–V) one, eccentrically located within the ventral portion of the allantois, nearer to the visceral endoderm than to the amnion (Fig. 1I,H). Although the T-domain's borders were not well circumscribed (e.g., Fig. 1I), they were compact enough to estimate allantoic T's longitudinal breadth (Fig. 3A). The T-defined core achieved its greatest average length by the LHF stage, after which it remained relatively constant (Fig. 3A). Oct-3/4–positive cells overlapped the T-domain at all stages (Downs, 2008) (Fig. 1J, Fig. 3A), but extended farther into the allantois before contracting.

The T-domain occupied approximately a third of the allantois' full length between headfold (HF) and 7-s stages (Fig. 3B, and data not shown). Although the T core's proportionate length was little changed by 6-s, the core itself was less uniformly positive (Fig. 4A). By 8-s, the dense allantoic core domain was still present, but was only slightly T-positive (Fig. 4B). By contrast, distal endothelial cells now contained T, as previously reported (In-man and Downs, 2006a). Additionally, a small strip of proximal ventral mesothelium contained cytoplasmic T while many cells of the nearby invaginating hindgut contained nuclear T, as previously described (Wilkinson et al., 1990;Inman and Downs, 2006a; Fig. 4B).

Transverse sections through the allantois suggested that reduction in the girth of the T core was due to widespread differentiation of T-positive cells into Flk-1 vascular components, ostensibly breaking up the compactness of proximal core cells. Similar to Oct-3/4 (Downs, 2008), some T-positive cells colocalized with Flk-1 along the length of the allantois (≥EHF stages), being most conspicuous by 3-s in the mid-region relative to the proximal one (Fig. 4C). By 4-s, T/Flk-1–positive cells were more evident in the base of the allantois (data not shown), supporting previous observations that differentiation of allantoic mesoderm into Flk-1 angioblasts occurs with distal-to-proximal polarity over time (Downs et al., 1998, 2004). By 6-s, abundant vascular elements were observed in the T-positive core, many of which were T/Flk-1– positive (Fig. 4D).

On the basis of these observations, we tentatively conclude that the posterior primitive streak spans the embryonic/ extraembryonic midline of the mouse conceptus. From the extraembryonic component, the allantois emerges. This extraembryonic primitive streak, the XPS, expanded into a T-defined Allantoic Core Domain, henceforth referred to as the ACD, which is composed of relatively undifferentiated cells that also contain Oct-3/4. The length of the ACD became stable by the LHF stage, and remained relatively unchanged during the period of allantoic elongation and vascularization; many of its cells ultimately became part of the nascent umbilical vasculature.

The ACD Does Not Reform After Microsurgical Removal (≥EHF stages)

We had demonstrated that the T-defined allantoic core died in T^C/T^C mutants (Inman and Downs, 2006b), leaving behind short T^C/T^C allantoises that invariably failed to elongate to fuse with the chorion. In other experiments, we had shown that microsurgical removal of wild-type allantoises resulted in short allantoic "regenerates," most of which failed to reach the chorion to form the placenta (Downs et al., 2004). However, as the ACD had not yet been discovered, its status was not known in these wild-type regenerates. Therefore, we tested the hypothesis that the factor required for allantoic elongation in the wild-type regenerates was the T-defined ACD.

As a first step toward exploring this possibility, allantoises were removed from conceptuses at each of the early bud (EB) -5-s stages. Immediately after microsurgery, some conceptuses were fixed and immunostained, which verified that most of the allantois had been removed (Fig. 5A–D). Next, operated conceptuses were cultured alongside unoperated ones for 3–12 hr; short culture periods ensured that final allantoic stages were between HF and 6-s, when T localized to the ACD (Fig. 3A). No matter how small or large the allantois at the time of its aspiration, all resulting allantoises were considered after culture to be "regenerates." Unoperated allantoises and −ACD allantoic regenerates (−ACDrg; EB, LB: N = 4; EHF, LHF: N = 13; 1–2-s: N = 3; 3–5-s: N = 4) were examined for the presence of T after culture (median, average final stage: 4-s). The ACD was present in 4/4 −ACDrg created at EB and LB stages (e.g., Fig. 5E), and in 2/10 EHF −ACDrg (Fig. 5F). By contrast, the ACD was absent in 8/10 EHF −ACDrg (Fig. 5G) and in 10/10 −ACDrg created thereafter (data not shown). In a similar set of experiments, we investigated Oct-3/4's status in −ACDrg (LB: N = 3; LHF: N = 1; 2-s: N = 2; 3-s: N = 5; 4–5-s: N = 2) after appropriate culture (median, average final stage: 5-s). All LB-stage-initiated −ACDrg exhibited an Oct-3/4 −positive core (compare Fig. 5H,I), while those initiated at ≥LHF stages lacked it (e.g., Fig. 5J, and data not shown), demonstrating that Oct-3/4–positive cells are part of the ACD.

Application of 1,1′, di-octadecyl-3,3,3′,3′,-tetramethylindo-carbocyanine perchlorate (DiI) to the central region of the IPS before removing allantoises (≥EHF stages; N = 3 experiments) confirmed that −ACDrg are derived, at least in part, from the IPS, as all −ACDrg contained labeled cells (data not shown). Only a few caspase-3–positive dead cells (≤10) were ever found in allantoises of freshly dissected specimens at all stages under study, which were restricted to the central allantoic region along its length by HF stages (data not shown; see the Experimental Procedures section). We have no reason to believe that apoptosis plays a role in failure of the regenerates to elongate.

The ACD Is Essential for Allantoic Elongation

The aforementioned results suggest that the ACD is essential for elongation. To test this hypothesis, we compared −ACD regenerates with those in which the proximal ACD-containing region was left intact. First, as such manipulations would be carried out in living specimens, and the length of the T-defined ACD had been determined in fixed material (Fig. 3A), we estimated the length of the fresh ACD by calculating the amount by which it shrank at each stage after fixation/immunostaining (Fig. 6A; see the Experimental Procedures section). On that basis, for "+ACD" conceptuses, we left intact approximately 133 μm of the base of the allantois (Fig. 6B); +ACD conceptuses were cultured alongside −ACD and unoperated ones (Fig. 6C,D), described in the previous section. All allantoises and allantoic regenerates were examined after 20 hr of culture (Fig. 6E).

To minimize the number of animals used in this part of the study, we combined results of previous −ACDrg experiments (Downs et al., 2004) with results here. Approximately 80 percent of 20-hr −ACDrg created at the EB stage grew far enough to fuse with the chorion

(Fig. 7A). By LB and HF stages, when the ACD had almost achieved its full length (Fig. 3A), approximately 60–80 percent of −ACDrg failed to elongate far enough to fuse with the chorion (Fig. 7A). Thereafter, when the length of the ACD had stabilized and was mature, most (≥ 90 percent) −ACDrg did not elongate. By contrast, all unoperated allantoises and nearly all +ACD regenerates (+ACDrg) fused with the chorion (Fig. 7B). Those few +ACDrg that did not fuse (3/42) had been created at 4–5-s stages when many ACD cells were differentiating into blood vessels, ostensibly reducing the available pool for elongation (Fig. 4).

Although the lengths of +ACDrg and unoperated allantoises were similar at all stages, +ACDrg were shorter than might be expected when created at ≥2-s (Fig. 8A), which could be accounted for by the observation that, during normal development, the distal allantoic region spreads across the chorionic surface at ≥10-s (Basyuk et al., 1999;Downs, 2002). Furthermore, while growth differentials of +ACDrg were indistinguishable from unoperated controls at early stages (Fig. 8B; see the Experimental Procedures section), these differentials were markedly increased in +ACDrg created at later stages (2–5-s; Fig. 8B), when intact allantoises were normally quite long (Downs and Bertler, 2000). By contrast, all −ACDrg were generally shorter than normal (Fig. 8A), and exhibited decreased growth differentials prior to 2-s (Fig. 8B). By 2-s, both unoperated allantoises and -ACDrg exhibited attenuated growth (Fig. 8A).

Thus, +ACDrg and −ACDrg differed in their ability to elongate and fuse with the chorion. Elongation of regenerates correlated with the presence of the ACD. Increased growth differentials in +ACDrg compared with those of unoperated allantoises suggest that, when the distal region is removed, the ACD returns to a “ground state,” and begins the elongation process anew. In this way, information in the distal allantoic region may feed back onto the ACD to regulate allantoic size.

The ACD Is Not Required for Vascular Patterning in the Allantois

During the period of elongation, the allantois creates a vascular plexus, which is thought to be established de novo (Downs et al., 1998). Whereas Flk-1–positive elements and VCAM-1–positive distal mesothelium were present in both −ACDrg (Downs et al., 2004) and +ACDrg (data not shown), the status of vascular patterning, defined by Platelet Endothelial Cell Adhesion Molecule-1 (PECAM-1; Inman and Downs, 2006b) was not known. To examine patterning, we created allantoic regenerates (EHF-5s) and cultured them in medium containing rat serum alongside unoperated controls until 6–9-s, when the PECAM-1–positive vasculature could be visualized before tail rotation. In addition, regenerates were created between the LB and 1-s stages and cultured for 10 hr in fetal calf serum to verify results with a more robust PECAM-1 antibody, Mec13.3 which, as it had been raised in rat, could not be used in conceptuses cultured in standard culture medium containing 50% rat serum (Downs, 2006).

All unoperated (12/12), many +ACD (9/11) and −ACD (8/13) regenerates exhibited an appropriately patterned PECAM-1 vasculature that had fused with the embryonic dorsal aortae in register with the embryonic primitive streak (Fig. 6F–I, and data not shown). In some +ACDrg and −ACDrg, the PECAM vasculature was present, but was either not connected to the embryonic dorsal aortae (Fig. 6I) or appropriately organized (data not shown). Given the number of correctly patterned regenerates of both (−ACD and +ACD) types, abnormal patterning likely resulted from inadvertent microsurgical damage and improper “healing” of the regenerates, rather than a requirement for the ACD.

On the basis of these findings, we conclude that the signals required for allantoic vascularization, defined by the presence of endothelialized Flk-1–positive cells, and PECAM-1 patterning, do not emanate from the ACD. Moreover, vascularization, because it occurred in −ACDrg, which are generally foreshortened, is not required a priori for elongation.

The ACD Contributes Extensively to the Allantois; the IPS Contributes to the Proximal Flanks

The regenerate results suggest that the ACD is the allantoic element responsible for elongation to the chorion. However, because the proximal region contains both the ACD and flanking cells, we sought to clarify each region's contributions to the allantois. For this, DiI was applied to four regions: to the central ACD, to the left or right proximal allantoic flanks, and within the central IPS (Fig. 9A–C). Labeled conceptuses were cultured for 12 hr (EHF-5-s; N = 31; Fig. 9D–F) or 20 hr (EB-5-s; N = 103; Fig. 9G–I).

Between the EHF- and 5-s stages, descendants of the ACD formed a continuous file that extended from the site of application through the allantoic midline (Fig. 9D). By 20 hr, this file was elaborately branched, spreading throughout the distal region (Fig. 9G; Table 1). By contrast, descendants of the nascent ACD at EB and LB stages ended up predominantly in the distal allantoic region, or scattered throughout the allantois, respectively (Table 1 and data not shown). A few initial DiI applications were > 133 μm from the ACD/IPS boundary (3/43; Table 1); their descendants formed a circumferential band beneath the chorioallantoic fusion junction (data not shown).

Nearly all DiI applications to the left or right proximal flanks remained as a generally cohesive unit, either remaining in place (29.2%) or translocating to the mid- (45.8%) or sometimes, distal (20.8%) allantoic flanks, always within the same labeling plane (Fig. 9E,H; Table 1). Thus, 75% of proximal flanking cells remained within the proximal half of the allantois. Descendants of half of all applications to the IPS remained solely within the posterior embryonic region, while the other half contributed to both the posterior embryonic region and the proximal flanks of the allantois (Fig. 9F,I; Table 1) or to the proximal flanks of the allantois alone (Table 1). Although DiI-labeled specimens were not sectionally analyzed, we deduce that IPS-derived cells surround the ACD, rather than become part of it; otherwise, they, too, would have been included in the midline file through the allantois, and this was never observed.

These results suggest that, by the EHF stage, the ACD contains a self-maintaining cell reservoir that contributes extensively to the proximal central core and distal half of the allantois in register with the embryonic body axis, resembling the PECAM-1– patterned vasculature. By contrast, contributions from the IPS were solely to its proximal flanks, and were not patterned with respect to the embryonic body axis. Moreover, IPS descendants did not always enter the allantoic compartment.

Thus, these results support the +ACD and −ACD regenerate studies, above, which suggest that the ACD is the major source of allantoic cells, and that these are essential for elongation. By contrast, the IPS is a minor source of cells, which are not capable of restoring elongation to allantoises lacking the ACD.

Wild-Type ACD Tissue Is Capable of Elongating But Not Fusing to the Chorion When Transplanted Into the T^C/T^C Environment

Grafting experiments further clarified the properties of the proximal region. 133 μm of the Rosa26/+ -labeled proximal region ("+ACD" grafts) was synchronously placed, by means of a hole made in the AX, into individual unlabeled host conceptuses from which the allantois had been removed (Fig. 10A). Four other similar-sized regions located on either side of the proximal allantois, the IPS, embryonic mid-primitive streak (MPS), and the distal and mid-allantoic regions, were also grafted into the same site (Fig. 10A).

Each type of graft produced different outcomes. At all stages, descendants of +ACD grafts contributed extensively to the allantois along its full length, forming a proximal central file that fanned out and encompassed the distal half (Fig. 10B,C; Table 2). By contrast, the IPS contributed either to the tail bud, the proximal allantoic flanks, or to both (Fig. 10D; Table 2).

MPS descendants contributed only to the posterior tail bud, and did not enter the allantois (Fig. 10G). Grafts of the distal and mid-allantois were spatially restricted to the distal and/or mid-regions, indicative of the regions' origin (Fig. 10E,F; Table 2; Downs and Harmann, 1997). PECAM-1 immunostaining a subset of +ACD chimeric allantoises confirmed the presence of the patterned vasculature in the +ACD chimeras (Fig. 10H,I).

Given the role of the ACD in allantoic elongation, we had expected a more striking difference between the lengths of chimeric allantoises bearing the ACD graft and those without it. Although +ACD chimeric allantoises tended to be longer than all others (Table 2), this difference was just significant at HF stages ($P = 0.05$) and significant at 1–4-s ($P = 0.004$). As no effort had been made to maintain the orientation of the ACD during grafting, these results suggest that the ACD may be compartmentalized into anterior and posterior regions. It is possible that those +ACD grafts that were not properly oriented could not restore elongation in a timely manner. Alternatively, progenitor cells present in older ACD grafts are rapidly differentiating, thereby limiting the supply of cells used for elongation (Fig. 4).

With those caveats, we tested the ability of the ACD to restore elongation to T^C/T^C mutant allantoises. As $T^C/+$ animals do not efficiently produce a copulation plug (Inman and Downs, 2006b), it was not an easy feat to obtain synchronous donor and host conceptuses. Nevertheless, several stage-matched litters were achieved. We had previously demonstrated that the IPS of T^C/T^C mutant embryos contributed cells to the allantois (Inman and Downs, 2006b). Here, we verified that, after removal of the T^C/T^C allantois, a T^C/T^C allantoic remnant formed after 6 h and was similar to the wild-type −ACD regenerate (compare Fig. 11A,B). This agrees with our previous finding that the IPS behaves normally until 1-s (Inman and Downs, 2006b). However, 12-h T^C/T^C −ACDrg did not seem to elongate further (compare Fig. 11C,D), suggesting that the IPS is ultimately defective in contributing further to the allantois.

Unoperated EHF wild-type and T^C/T^C conceptuses (Fig. 11E–F′) were cultured alongside EHF wild-type and T^C/T^C conceptuses that had received a synchronous graft of the donor wild-type proximal allantoic region after removal of the host allantois (Fig. 11G–H′; Table 2). As predicted from the aforementioned regenerate results, T^C/T^C mutant host cells contributed to the proximal allantois of chimeric allantoises, while wild-type donor cells were present everywhere but the proximal flanks (Fig. 11H,H′). Furthermore, although chimeric allantoises exhibited lengths similar to wild-type controls (Fig. 10; Table 2), they did not unite with the chorion, possibly because the grafts were not appropriately oriented, as described above, or because this event requires T, which is also found in the chorion (Inman and Downs, 2006a) but was absent in mutant hosts (Inman and Downs, 2006b).

Collectively, results of grafting, in situ fate mapping and regenerates demonstrate that the ACD is essential for allantoic elongation. No other transplanted tissue of similar size and origin was capable of promoting allantoic elongation when grafted into the host conceptus. Additionally, the wild-type ACD tissue was able to create an elongated chimeric allantois in the mutant environment. Thus, the ACD is a distinct domain that is responsible for allantoic elongation and contributes significant numbers of cells to the developing umbilicus.

AX May Collaborate With the Extraembryonic Primitive Streak to Establish the ACD

Our data demonstrate that the length of the ACD is stable by HF stages (Fig. 3A). If allantoises are removed before this time, the ACD is generally, but not always, present, but if removed thereafter, most allantoic regenerates lacked the ACD and did not elongate. It has been known since the studies of Bonnevie (Bonnevie, 1950), that visceral endoderm at the embryonic/extraembryonic boundary of the mouse conceptus, is transitional in morphology between the columnar extraembryonic visceral endoderm of the yolk sac, and the squamous visceral endoderm overlying the embryo.

During the time period under examination, we observed that the transitional visceral endoderm which overlies the allantois, and which we refer to here as the allantois-associated extraembryonic visceral endoderm, the AX, exhibited intriguing properties. Before HF stages, cells within the AX were cuboidal, contained cytoplasmic T (Fig. 1, Fig. 12A), abundant apical vacuoles, and long microvilli (Fig. 2K,L). In this way, the AX exhibited a cellular profile more similar to classic extraembryonic visceral endoderm than to embryonic visceral endoderm (Haar, 1970;Haar and Ackerman, 1971). By the EHF stage, the proximal region of the AX was becoming more squamous and many of its cells lost cytoplasmic T (Fig. 12B); now, when present, T localized to the nucleus (Fig. 1G, Fig. 12B). Moreover, the more squamous proximal AX contained fewer vacuoles and exhibited shorter and less abundant microvilli (Fig. 2M). By early somite stages, the AX was fully squamous and contained few, if any vacuoles and shorter, more widely spaced microvilli (Fig. 2N,O). Many T-positive nuclei were observed within it (Fig. 3C).

Calculations of the ratio of proximal AX containing nuclear T:distal AX containing cytoplasmic T was 0–20% at the EHF stage (N = 14). Thereafter, this ratio increased with developmental stage: LHF: 40–100% (N = 6); 1-s: 50– 100% (N = 4); 2-s: 75–100% (N = 5); and 3–6-s, 100% (N = 28). Thus, over time, the AX lost cytoplasmic T, vacuoles, and microvilli, and became reduced in height, with some cells exhibiting nuclear T.

Intriguingly, the timing of appearance of nuclear T in the AX coincided with that of Oct-3/4 (Downs, 2008; Fig. 3C), and numbers of T- and Oct-3/4-positive cells fluctuated in relative synchrony with developmental stage (Fig. 3C). By the 8-s stage, the allantois was no longer directly associated with the AX; rather, its length was apposed to the yolk sac, and separated by the exocoelom (Fig. 4B). Together, these results demonstrate that the morphological and immunohistochemical profile of the AX changes over time.

Based on these observations, we hypothesized that the AX is involved in establishment and/or maintenance of the ACD. To test this possibility, allantoises were removed from conceptuses (EB-5-s) and explanted with or without the associated AX. Measuring allantoises before and after explantation allowed direct matched comparisons (Fig. 13A – H). Villin, which identified visceral and hindgut endoderm (Pinson et al., 1998; Fig. 13I,J), verified the presence of the AX in the explants (Fig. 13K,L).

Not only did all allantoic explants survive culture (Table 3), but the AX survived at all stages, forming a cyst-like structure, typical of visceral endoderm (Copp et al., 1986) (Fig. 13K). At the EB stage, +AX explants were slightly, but not significantly, larger than −AX explants (Fig. 13A,B;Table 3). By the LB stage, +AX explants were significantly larger, exhibiting many unvascularized cells (Fig. 13C,D;Table 3). By HF stages, +AX and −AX explants were indistinguishable, exhibiting a mound of relatively undifferentiated cells (Fig. 13E–H;Table 3) which, as shown in a previous study (Downs et al., 2001), identifies the proximal allantoic region in explant culture. The remainder of the explant was highly vascularized. Although we attempted to count allantoic cells, the AX was so closely juxtaposed to the allantois, particularly at early stages (Fig. 2K – O), that aspirating it resulted in loss of associated allantoic cells. Nevertheless, these preliminary data suggest that, at the bud stages, the AX collaborates with the extraembryonic primitive streak to establish the ACD.

DISCUSSION

The Murine Primitive Streak Creates Two Germinal Centers, Extraembryonic and Embryonic, to Build Distinct Allantoic Compartments

In this study, we investigated the relationship between the allantois and the primitive streak. Our findings are summarized in Figure 14. At the OB stage, the posterior end of the primitive

streak extended into the extraembryonic region as a wedge of densely packed cells that contained T and were morphologically identical to the T-positive IPS (Fig. 14A). As the neural plate stages progressed, the allantoic bud emerged near the distal-most extension of the XPS (Fig. 14B). Thereafter, the XPS expanded into a fully mature T-defined ACD, possibly by influence from the overlying AX (Fig. 14C). The cells of the ACD were loosely organized, and exhibited a relatively undifferentiated ultrastructural profile. At maturity, ACD descendants colonized all but the proximal flanks of the allantois (Fig. 14D – F), creating a patterned midline structure in register with the embryonic primitive streak (Fig. 14F) that fanned throughout the distal region. By contrast, contribution from the IPS to the allantois was modest; IPS descendants localized to the allantoic proximal flanks (Fig. 14F).

Together, these data suggest that the posterior primitive streak does not terminate abruptly within the embryo proper, but extends its reach into the exocoelom. Although this conclusion challenges conventional wisdom concerning the physical limit of the primitive streak, posterior streak extension and transformation into the ACD took place over a brief 4–8 hr window, a period that had been excluded from analysis by Sobotta. Thus, this fundamental property of the primitive streak was undoubtedly missed.

Although we cannot rule out the possibility that T-expressing cells in the OB exocoelom represent nascent mesoderm that has moved away from its site of origin in the proximal embryonic streak epiblast, we believe this is unlikely. First, two other gene products involved in axial specification, Hoxb1 and Hoxb8, are both present at the OB-LB stages in the extraembryonic extension of the streak described here (Deschamps and Wijgerde, 1993; Deschamps et al., 1999; Forlani et al., 2003). Second, the cells of the extraembryonic and intraembryonic components of the primitive streak were ultrastructurally identical, with both populations localized to the midline of the conceptus. Third, the XPS-established ACD produced a midline file of cells in register with the embryonic body axis, or primitive streak, revealing that the XPS, and not the IPS, is part of the A–P axis that contains patterning information.

It is generally assumed that the primitive streak is established by the loosening of epithelial contacts within the midline of the epiblast, in an epithelial-to-mesenchymal transformation (EMT; Hashimoto and Nakatsuji, 1989). Our conclusions are not at odds with an EMT event; embryonic epiblast may undergo this transition, after which the streak translocates into the extraembryonic region. Alternatively, ectoderm of the egg cylinder spans both the embryonic and extraembryonic regions. Perhaps, at the onset of gastrulation, the EMT that forms the streak spans both regions, too. This possibility is supported by expression of *Brachyury* in both the embryonic and extraembryonic ectoderm on one side of the egg cylinder just prior to gastrulation (Rivera-Perez and Magnuson, 2005).

On the basis of these observations, we suggest that the murine primitive streak is germinally symmetric at both ends: the anterior streak's ventral node contains a cell reservoir that extends the rostral body axis further anteriorly through the notochord (Lawson et al., 1991; Beddington, 1994; Kinder et al., 2001; Cambray and Wilson, 2007), and the posterior streak's ventrally located ACD contains a progenitor pool that extends the caudal body axis further posteriorly by means of the core of the allantois (this study). This notion is supported experimentally by ablation studies: ablation of the node resulted in truncation of the body axis (Davidson et al., 1999), while ACD ablation truncated the allantois (this study). Moreover, like the node (Beddington, 1994), the ACD alone produced a midline file of cells in register with the embryonic primitive streak, revealing that it, and not the IPS, contains axial patterning information. It is intriguing that several protein products, Wnt11 and Bmp7 (Kispert et al., 1996; Arkell and Beddington, 1997), the latter of which is involved in allantoic development

(Solloway and Robertson, 1999) are discretely expressed in just these two structures during gastrulation, with no expression in between.

That the posterior primitive streak lies within the exocoelom and establishes the allantois strongly suggests that the embryonic body axis and allantois are continuous morphological features, and solves the riddle of why, in some genetic mutants, both the allantois and embryonic axis are foreshortened or duplicated (Inman and Downs, 2007). A primitive streak that spans the posterior embryonic and extraembryonic compartments likely endows them with a common set of spatial coordinates, unifying embryonic and extraembryonic tissues through a common midline.

To what biological purpose could a continuous A–P system of coordinates serve? It is little appreciated that the primary umbilical artery and its connection to the embryonic dorsal aorta lie in register with the primitive streak (Inman and Downs, 2007). Little is known about this connection, but remodeling it (Gest and Carron, 2003) involves axial information. In the only example of which we are aware, the left and right umbilical arteries of sirenomelia mutant embryos are replaced by a single one that is misaligned onto the embryonic midline aorta (Schreiner and Hoornbeek, 1973). We hypothesize that the extraembryonic component of the primitive streak coordinates this connection, possibly through activity of the Hox genes found there (Deschamps and Wijgerde, 1993; Deschamps et al., 1999), and/or by means of *Lpp3*, whose loss leads to axial and extraembryonic vascular defects (Escalante-Alcalde et al., 2003). Labeled ACD descendants produced a pattern that resembled the nascent PECAM-1 vasculature (Inman and Downs, 2006b), but it is not yet known whether these represent the same structure, especially as the PECAM-1 vasculature was present in the absence of the ACD. Clearly, our results represent only the beginning of intense investigation into the complexity of the posterior region.

AX May Induce Formation of the ACD

Visceral endoderm is a potent inducing tissue, required for chick and murine yolk sac hematopoiesis and vascularization (Wilt, 1965; Belaoussoff et al., 1998). In addition, AVE patterns neurectoderm (Thomas and Beddington, 1996). The morphological, molecular, and behavioral profiles of the AX suggested diverse roles in development of the posterior region.

Results of the allantoic explant studies suggested that the AX is involved in expansion of the XPS into the ACD. During the allantoic bud stages, the AX contained cytoplasmically localized T. Cytoplasmic T is not an immunostaining artifact, as results of other studies have demonstrated that interaction between T and the nuclear export signal, CRMI, resulted in T's translocation from the nucleus (Kulisz and Simon, 2008). Although the significance of cytoplasmic T is not known, Tbx5, another member of the T-box family of transcription factors, is shuttled between the nucleus and cytoplasm in a variety of cell types during cardiogenesis (Bimber et al., 2007). This suggests a generalized paradigm of protein subcellular localization in T-box-mediated differentiation.

By the time the ACD matured, the AX was flattening and becoming less vacuolated; many of its cells exhibited nuclear, rather than cytoplasmic, T. Intriguingly, the appearance of nuclear T- overlapped that of Oct-3/4. Synchronous appearance of T- and Oct-3/4–positive cells in the AX may reflect similar proliferation/differentiation and movement within the two populations. Although their origin and fate are not known, one possibility is that T- and Oct-3/4–positive AX cells originate within the ACD and will become part of the hindgut endoderm, as both T (Herrmann, 1991; Inman and Downs, 2006a) and Oct-3/4 (Downs, 2008) were found there. Another possibility is that some are primordial germ cells (PGCs), as PGCs temporarily reside within the base of the allantois (Ozdzenski, 1967; Ginsburg et al., 1990) before translocating into hindgut endoderm and migrating to the gonads.

The ACD: A Stem Cell Niche?

As cells of the ACD contribute to the umbilical vasculature, and possibly become migrating PGCs, hindgut endoderm, and even, as shown recently, definitive hematopoietic cells (Zeigler et al., 2006), it is tantalizing to speculate that the ACD is a stem cell niche for a variety of cell types. The ultrastructural profile of the ACD cell population, together with the presence of Oct-3/4 (Palmieri et al., 1994; Downs, 2008), which is found in relatively undifferentiated cells and the germ line (Scholer et al., 1990), support the notion that the ACD contains a progenitor cell population. Previous results of heterotopic grafting experiments demonstrated that descendants of proximal allantoic cells colonized derivatives of all three primary germ layers (Downs and Harmann, 1997; Downs, 1998).

The source of cell lineage sorting signals is not known. However, as −ACD regenerates contained Flk-1 vascular elements (Downs et al., 2004) and a PECAM-1 patterned vasculature, despite the absence of the ACD, the cues that establish the umbilical vasculature must lie outside the ACD. Given that a few regenerates were not perfectly patterned, the AX is one possible source of these signals, as it is juxtaposed to the allantois and is likely to be damaged or disturbed during microsurgical manipulation. Also, as described in the previous section, visceral endoderm is a potent inducing tissue for hematopoiesis and vascularization.

Does the ACD Regulate Allantoic Size?

Several observations suggest that the ACD may regulate allantoic size. Removal of the distal portion of the allantois at later stages resulted in significant “catch-up” growth relative to unoperated and −ACD regenerated allantoises, revealing that the ACD is capable of enhanced growth. Thus, information within the distal region may feed back onto the ACD, regulating allantoic elongation (Fig. 14). Furthermore, during the period of allantoic elongation, proximal flanking cells sometimes remained in place, while IPS cells often stayed within the embryonic region. In other cases, flanking cells ended up distally, while IPS descendants ended up in the proximal allantois. These patterns suggest that influx of cells from the IPS into the allantois is regulated, possibly by direct communication between the ACD and IPS. Alternatively, the ACD may indirectly regulate cell flow from the IPS, controlling the rate of proliferation in flanking IPS-derived cells once they have entered the allantois, and placing a hold on subsequent IPS contributions.

The molecular mechanisms through which the ACD controls size are not clear, but the MI was significantly reduced in T^C/T^C mutant allantoises (Inman and Downs, 2006b), highlighting a role for T in regulating cell proliferation. In addition, Mxl1 was found in the base of the allantois (EB-EHF stages) (Pearce and Evans, 1999); loss of Mxl1 resulted in deregulation of allantoic size, and a greatly enlarged allantois in Mxl1 mutants (Hart et al., 2002), further suggesting that the ACD regulates allantoic size.

Origin of the Allantoic Bud

On the basis of morphological observations, the murine allantois is thought to be composed wholly of mesoderm (Duval, 1891). The rodent allantois is therefore different from most other mammalian umbilical precursors which also contain an endodermal component (Mossman, 1937). However, whereas results here have not resolved this difference in the animal kingdom and thus, await future studies, they do challenge the traditional view that mesoderm, both embryonic and extraembryonic, is created by transformation of epiblast through the primitive streak (Beddington, 1983). Together with So-botta’s conclusions, it is assumed that the allantoic bus is established by IPS-derived mesoderm that is displaced into the extraembryonic region.

Whilst ingression of epiblast through the primitive streak undoubtedly ends up as mesoderm (Lawson et al., 1991), studies in other mammals, notably the armadillo (Enders, 2002), the macaque (Enders, 2007), and humans (Bianchi et al., 1993), exhibit extraembryonic mesoderm before the formation of the primitive streak. Thus, the streak is not a priori required for mesoderm formation. Several fate mapping studies of the IPS revealed that it contributes cells to the allantois (Tam and Beddington, 1987; Kinder et al., 1999), but they provided no evidence that the allantoic bud itself is established by it.

Our results suggest that the allantoic bud emerges from the distal portion of the XPS, and is initially discontinuous with the IPS. Then, as the more proximal portion of the XPS expands (Fig. 14), the allantois merges with the IPS. The mechanism by which bud mesoderm forms is not known, but at least two “nontraditional” scenarios which do not involve transformation of epiblast through the IPS may be envisioned. In the first, the XPS, together with the AX, creates a “survival site” for the formation of the allantoic bud. The bud would be composed of extraembryonic mesoderm that has not yet cavitated to form the exocoelom. Such a survival center was proposed by Bonnevie (Bonnevie, 1950), though its precise whereabouts were not specified. Furthermore, the origin of the extraembryonic mesoderm that cavitates to form the exocoelom is not known. Alternatively, the XPS itself may create the allantoic bud de novo. The nascent allantois exhibited round T-positive cells throughout its length, which may have come from the XPS at the base (Fig. 1). Thereafter, once the ACD formed, proliferation within it would continue to build the core of the allantois.

The ACD: A Self-maintaining Germinal Center?

Thus, the ACD may not only regulate allantoic size by influencing nearby cell proliferation but, as suggested above, it may itself be a self-maintaining proliferative center. That DiI-labeled cells both remained at the site of application within the ACD and also elaborated a midline file support this suggestion. In addition, if removed, the ACD did not regenerate. Consequently, the regenerates were composed of flanking cells, derived from the IPS, which had limited elongation potential.

Strictly speaking, a proliferative center is defined by elevated levels of cell division within a specific cellular domain (Snow, 1978). At present, the proliferative index of the XPS and ACD are not known. Previous calculations of the mitotic index (MI) of the allantois did not uncover enhanced figures in the base of the allantois (Downs and Bertler, 2000). However, as the MI of the ACD and flanks were not distinguished, it is possible that a lower MI in the flanks may cancel an elevated one in the ACD, ensuring steady growth. Alternatively, as the MI was calculated in that part of the allantois above its site of insertion into the amnion and yolk sac, the critical region of the ACD may have been excluded from previous calculations. Thus, until the proliferative profile of the ACD has been fully characterized, it may most accurately be considered a “germinal center”.

The full germinative potential of the XPS and its expansion into the ACD will require focus on its fate and dynamics, similar to tour-de-force studies in the node (Kinder et al., 2001; Cambray and Wilson, 2007). For example, the ACD’s longitudinal breadth changed little over time, but whether its diameter decreased in direct proportion to differentiation within this population is not yet known. The relative inaccessibility of the ACD within the proximal region compared with the node at the other end of the streak will make experiments such as these extremely technically challenging.

CONCLUSIONS

We conclude that the posterior region of the murine conceptus is more architecturally and functionally complex than has been previously appreciated. Findings here will serve as a point

of departure not only for elucidating the role of several gene products in whose absence the allantois does not grow far enough to fuse with the chorion to create the placenta (reviewed in In-man and Downs, 2007), but the posterior region of the mammalian conceptus as a whole, especially the relationship between the embryo and its placenta, whose establishment and interdependencies have been generally ignored.

EXPERIMENTAL PROCEDURES

Animal Husbandry, Embryo Dissections, Staging, and Whole Embryo Culture

Mouse strains B6CBAF1/J (The Jackson Laboratory, Bar Harbor, ME), ROSA26/26 (Downs and Harmann, 1997), T^{C}/+ (Inman and Downs, 2006b), and Kdr^{tm1Jrt} (Shalaby et al., 1995; Inman and Downs, 2006b) were used in this study. All littermates from T^{C}/+ intercrosses were genotyped as previously described (Inman and Downs, 2006b). Time-mated females were dissected (Downs, 2006) and staged (Downs and Davies, 1993). Embryos were cultured as previously described (Downs, 2006).

Terminology and Acronyms

The following terminology and acronyms were used in this study:

ACD, Allantoic Core Domain; −ACD, +ACD, general scenarios in which (1) the entire allantois was removed (−ACD), or (2) the distal allantoic region was removed, leaving the proximal ACD-containing region intact (+ACD); −ACDre, refers to conceptuses immediately after removal of the entire allantois (−ACDre); −ACDrg and +ACDrg, refer to the allantoic regenerates that form in culture after removal of (1) the entire allantois (−ACDrg), or (2) just the distal portion, leaving intact the proximal region containing the ACD (+ACDrg); al-c, are those chimeric allantoises created by grafting into the site where the entire allantois was removed; AX, allantois-associated extraembryonic visceral endoderm.

Morphological Stages (see also Downs and Davies, 1993; Downs, 2008)

OB, no allantoic bud stage (~7.0–7.25 dpc); EB, early bud stage (~7.25–7.5 dpc); LB, late bud stage (~7.5–7.75 dpc); vEHF, very early headfold stage (headfolds just visible; ~7.75 dpc); EHF, early headfold stage (7.75–8.0 dpc); LHF, late headfold stage (~8.0 dpc); -s, somite pairs >8.0 dpc; one somite pair is added to the file in culture conditions used here approximately every 90–120 min (Downs and Gardner, 1995).

TEM

For TEM (Fig. 2), conceptuses were prepared as described previously (Enders et al., 2006). Specimen numbers per stage/light microscope/TEM: OB: 2,1,1; EB: 2,2,2; LB: 4,4,4; LB/EHF: 4,4,2; vEHF: 4,4,2; EHF: 6,6,4; LHF: 2,2,2; 1-s: 5,5,4; 2-s: 3,3,3; 3-s: 6, 6,4; 4-s: 1,1,1; 5-s: 3,3,3.

Microsurgical Manipulations

Removal of whole allantoises (“−ACD”) (Fig. 5, Fig. 6) was carried out as previously detailed (Downs, 2006). “+ACD” manipulations (Fig. 6) kept intact the proximal ACD-containing region, and required a narrower micropipette to remove the distal and mid-allantoic regions only, to exclude the proximal region. To determine the length of the ACD in living specimens (Fig. 6A), the following set of steps was carried out. First, the length of the T-defined ACD was calculated in fixed/immunostained material (Fig. 3A). Then, we estimated by how much the allantois shrank after immunostaining by comparing the length of allantoises in their living and fixed/immunostained states (Fig. 6A). Allantoic “shrinkage factors” were then calculated for each stage between LB-5-s stages (Fig. 6A). The average length of each stage’s T-defined

ACD (Fig. 3A) was then multiplied by its cognate shrinkage factor, producing fresh ACD lengths that ranged from 141 to 211 μm, with an average of 158 μm. Given the natural contours of the allantois, in which the base of the allantois is considerably wider than its distal region (e.g., Fig. 9A), approximately 133 μm of the allantois was left intact after aspiration in +ACD studies.

Allantoic "length differentials" (Fig. 8) were calculated in the following way: the length of the allantois at the start of culture was subtracted from the length of fresh allantoises immediately after culture.

Rosa26/+ conceptuses provided +ACD grafts in transplantation experiments (Fig. 10, Fig. 11). Most grafts were synchronous but a few were stage-matched to within 2–4 hr. After incubation in trypsin/pancreatin (Downs and Harmann, 1997), conceptuses were transferred to dissection medium (Downs, 2006), the allantois was aspirated and glass scalpels were used to cut out the regions of interest, which were inserted through the AX into the posterior embryonic/extraembryonic junction of hosts whose own allantois had been removed via the anterior yolk sac.

Preparation of allantoic explants (Fig. 13) was as previously described (Downs et al., 2001); some included the AX, whose association with the allantois was maintained by opening the exocoelom with forceps and cutting out the allantois/AX with glass scalpels. The ±AX-associated allantoises were cultured as previously described (Downs, 2006).

Immunostaining and Calculating the Length of the Allantoic T-Domain and Surface Area of Chimeric Allantoises

Immunostaining for T, Oct-3/4, villin, and caspase-3 (SC-17743; SC-8628; SC-7672; Santa Cruz Biotechnologies; and 557035, BD Biosciences/Pharmingen; respectively), were carried out as previously described (Downs, 2008). "Minus antibody" and control peptides (villin, SC-7672P) verified antibody specificity (Downs, 2008). PECAM-1 immunostaining was as previously described (Inman and Downs, 2006b), using monoclonal Armenian hamster anti-mouse PECAM-1 (2H8) (MAB-1938Z, Chemicon) on conceptuses cultured in rat serum, and the rat monoclonal Mec 13.3 antibody (557355; BD/ Pharmingen) on conceptuses cultured for 10 hr in medium containing 50% fetal calf serum, which permitted normal development (K. Downs, unpublished). Immunostaining allantoic explants was carried out as previously described (Downs et al., 2001). All antibodies were diluted 1/100. The length of the T-domain was estimated as for Oct-3/4 (Downs, 2008). In grafts involving $T^{Curtailed}$, the area of reconstituted chimeric allantoises was calculated by outlining sagittally oriented allantoises in whole-mount preparations using Metavue.

DiI Fate Mapping

A small volume (~0.5 μl) of 0.05 mg/ml CellTracker CM-DiI (1,1′dioctadecyl-3,3,3′,3′-tetramethylindo-carbocyanine perchlorate, Molecular Probes) in 0.3 M sucrose was applied to the central proximal ACD, its left or right flank, or the intraembryonic posterior primitive streak as previously described (Beddington, 1994). Bright-field and fluorescence images were taken immediately after application. For each specimen, x, y coordinates were calculated, with 0.0 being the midline of the boundary of the allantois/primitive streak. In that way, the proximal region of the ACD and IPS were subdivided into proximal left, mid, and right areas. A subset of conceptuses was injected and processed for histology to verify accuracy of dye application (Beddington, 1994). Fluorescent images were taken using a Spot RT-Slider camera (Diagnostic Instruments) attached to a Nikon Diaphot inverted microscope with a G2A filter cube (excitation 535, emission 590, Chroma Technology Corporation) and Metavue (Molecular Devices) software. Fluorescent images were pseudocolored in Metavue Software and

superimposed with brightfield images using Photoshop 7.0 software. In some cases, the location of the labeled descendants was verified by microdissection of the allantois, primitive streak, and visceral yolk sac.

Statistical Methods

For all experiments, $N \geq 3$ specimens for each stage, genotype, and manipulation presented, unless otherwise noted. All statistical analyses used the Student's two-way *t*-test, equal variances assumed (Mini-Tab), significance $P \leq 0.05$.

Acknowledgments

K.M.D. is grateful to Professor Robert Auerbach for translating the appropriate passages of Sobotta (1911). We thank Maria Mikedis and the anonymous reviewers for their constructive comments on the manuscript. Parts of this study were carried out in partial fulfillment of the Ph.D. degree in the Cellular and Molecular Biology Graduate Program (K.E.I.). K.M.D. was funded by a grant from the National Institutes of Child Health and Development.

Grant sponsor: the National Institutes of Child Health and Development; Grant number: RO1 HD042706

REFERENCES

Arkell R, Beddington RS. BMP-7 influences pattern and growth of the developing hindbrain of mouse embryos. Development 1997;124:1–12. [PubMed: 9006062]

Basyuk E, Cross JC, Corbin J, Nakayama H, Hunter PJ, Nait-Oumesmar B, Lazzarini RA. Murine Gcm1 gene is expressed in a subset of placental trophoblast cells. Dev Dyn 1999;214:303–311. [PubMed: 10213386]

Beddington, RSP. The origin of the foetal tissues during gastrulation in the rodent. In: Johnson, MH., editor. Development in mammals. Amsterdam: Elsevier Science Publishers; 1983. p. 1-32.

Beddington RSP. Induction of a second neural axis by the mouse node. Development 1994;120:613–620. [PubMed: 8162859]

Beddington RSP, Robertson EJ. Axis development and early asymmetry in mammals. Cell 1999;96:195–209. [PubMed: 9988215]

Belaoussoff M, Farrington SM, Baron MH. Hematopoietic induction and respecification of A–P identity by visceral endoderm signaling in the mouse embryo. Development 1998;125:5009–5018. [PubMed: 9811585]

Bianchi DW, Wilkins-Haug LE, Enders AC, Hay ED. Origin of extraembryonic mesoderm in experimental animals: relevance to chorionic mosaicism in humans. Am J Med Genet 1993;46:542–550. [PubMed: 8322818]

Bimber B, Dettman RW, Simon HG. Differential regulation of Tbx5 protein expression and sub-cellular localization during heart development. Dev Biol 2007;302:230–242. [PubMed: 17045582]

Bonnevie K. New facts on mesoderm formation and proamnion derivatives in the normal mouse embryo. J Morphol 1950;86:495–546.

Cambray N, Wilson V. Two distinct sources for a population of maturing axial progenitors. Development 2007;134:2829–2840. [PubMed: 17611225]

Copp AJ, Roberts HM, Polani PE. Chimaerism of primordial germ cells in the early postimplanatation mouse embryo following microsurgical grafting of posterior primitive streak cells in vitro. J Embryol Exp Morphol 1986;95:95–115. [PubMed: 3641878]

Crossley PH, Martin GM. The mouse Fgf8 gene encodes a family of polypeptides and is expressed in regions that direct outgrowth and patterning in the developing embryo. Development 1995;121:439–451. [PubMed: 7768185]

Davidson BP, Kinder SJ, Steiner K, Schoenwolf GC, Tam PP. Impact of node ablation on the morphogenesis of the body axis and the lateral asymmetry of the mouse embryo during early organogenesis. Dev Biol 1999;211:11–26. [PubMed: 10373301]

Deschamps J, Wijgerde M. Two phases in the establishment of HOX expression domains. Dev Biol 1993;156:473–480. [PubMed: 8096483]

Deschamps J, van den Akker E, Forlani S, de Graaff W, Oosterveen T, Roelen B, Roelfsema J. Initiation, establishment and maintenance of Hox gene expression patterns in the mouse. Int J Dev Biol 1999;43:635–650. [PubMed: 10668974]

Dobrovolskaia-Zavadskaia N. Sur la mortification spontanee de la queue chez la souris nouveau-nee et sur l'existence d'un charactere heriditaire "non-viable". C R Soc Biol 1927;97:114–116.

Downs KM. The murine allantois. Curr Top Dev Biol 1998;39:1–33. [PubMed: 9475996]

Downs KM. Early placentation in the mouse. Placenta 2002;23:116–131. [PubMed: 11945078]

Downs KM. In vitro methods for studying vascularization of the murine allantois and allantoic union with the chorion. Methods Mol Med 2006;121:241–272. [PubMed: 16251748]

Downs KM. Systematic localization of Oct-3/4 to the gastrulating mouse conceptus suggests manifold roles in mammalian development. Dev Dyn 2008;237:464–475. [PubMed: 18213575]

Downs KM, Bertler C. Growth in the pre-fusion murine allantois. Anat Embryol (Berl) 2000;202:323–331. [PubMed: 11000283]

Downs KM, Davies T. Staging of gastrulation in mouse embryos by morphological landmarks in the dissection microscope. Development 1993;118:1255–1266. [PubMed: 8269852]

Downs KM, Gardner RL. An investigation into early placental ontogeny: allantoic attachment to the chorion is selective and developmentally regulated. Development 1995;121:407–416. [PubMed: 7768182]

Downs KM, Harmann C. Developmental potency of the murine allantois. Development 1997;124:2769–2780. [PubMed: 9226448]

Downs KM, Gifford S, Blahnik M, Gardner RL. The murine allantois undergoes vasculogenesis that is not accompanied by erythropoiesis. Development 1998;125:4507–4521. [PubMed: 9778509]

Downs KM, Temkin R, Gifford S, McHugh J. Study of the murine allantois by allantoic explants. Dev Biol 2001;233:347–364. [PubMed: 11336500]

Downs KM, McHugh J, Copp AJ, Shtivelman E. Multiple developmental roles of Ahnak are suggested by localization to sites of placentation and neural plate fusion in the mouse conceptus. Mech Dev 2002;119S:S31–S38. [PubMed: 14516657]

Downs KM, Hellman ER, McHugh J, Barrickman K, Inman K. Investigation into a role for the primitive streak in development of the murine allantois. Development 2004;131:37–55. [PubMed: 14645124]

Duval M. Le placenta des rongeurs. Trosi'eme partie. Le placenta de la souris et du rat. J Anat Physiol Normales et Pathol de l'Homme et des Animaux 1891;27:24–73. 344–395; 515–612.

Enders AC. Implantation in the nine-banded armadillo: how does a single blastocyst form four embryos? Placenta 2002;23:71–85. [PubMed: 11869094]

Enders AC. Implantation in the macaque: expansion of the implantation site during the first week of implantation. Placenta 2007;28:794–802. [PubMed: 17188351]

Enders AC, Blankenship TN, Conley AJ, Jones CJP. Structure of the midterm placenta of the spotted hyena, Crocuta crocuta, with emphasis on the diverse hemophagous regions. Cells Tissues Organs 2006;183:141–155. [PubMed: 17108685]

Escalante-Alcalde D, Hernandez L, Le Stunff H, Maeda R, Lee HS, Gang-Cheng JR, Sciorra VA, Daar I, Spiegel S, Morris AJ, Stewart CL. The lipid phosphatase LPP3 regulates extra-embryonic vasculogenesis and axis patterning. Development 2003;130:4623–4637. [PubMed: 12925589]

Forlani S, Lawson KA, Deschamps J. Acquisition of Hox codes during gastrulation and axial elongation in the mouse embryo. Development 2003;130:3807–3819. [PubMed: 12835396]

Gest TR, Carron MA. Embryonic origin of the caudal mesenteric artery in the mouse. Anat Rec 2003;271:192–201.

Ginsburg M, Snow MHL, McLaren A. Primordial germ cells in the mouse embryo during gastrulation. Development 1990;110:521–528. [PubMed: 2133553]

Gluecksohn-Schoenheimer S. The development of normal and homozygous brachy (T/T) mouse embryos in the extraembryonic coelom of the chick. Proc Natl Acad Sci USA 1944;30:134–140. [PubMed: 16588636]

Gurtner GC, Davis V, Li H, McCoy MJ, Sharpe A, Cybulsky MI. Targeted disruption of the murine VCAM1 gene: essential role of VCAM-1 in chorioallantoic fusion and placentation. Genes Dev 1995;9:1–14. [PubMed: 7530222]

Haar JL. The visceral yolk sac of the mouse. A correlated phase contrast and electron microscopic study. Anat Rec 1970;166:311.

Haar JL, Ackerman GA. A phase and electron microscopic study of vasculogenesis and erythropoiesis in the yolk sac of the mouse. Anat Rec 1971;170:199–223. [PubMed: 4931266]

Hart AH, Hartley L, Sourris K, Stadler ES, Li R, Stanley EG, Tam PP, Elefanty AG, Robb L. Mixl1 is required for axial mesendoderm morphogenesis and patterning in the murine embryo. Development 2002;129:3597–3608. [PubMed: 12117810]

Hashimoto K, Nakatsuji N. Formation of the primitive streak and mesoderm cells in mouse embryos — detailed scanning electron microscopic study. Dev Growth Differ 1989;31:209–218.

Herrmann BG. Expression pattern of the Brachyury gene in whole-mount TWis/TWis mutant embryos. Development 1991;113:913–917. [PubMed: 1821859]

Inman K, Downs KM. Localization of Brachyury (T) in embryonic and extraembryonic tissues during mouse gastrulation. Gene Expr Patterns 2006a;6:783–793. [PubMed: 16545989]

Inman KE, Downs KM. Brachyury is required for elongation and vasculogenesis in the murine allantois. Development 2006b;133:2947–2959. [PubMed: 16835439]

Inman KE, Downs KM. The murine allantois: emerging paradigms in formation and development of the mammalian umbilical cord and its relation to the fetus. Genesis 2007;45:237–258. [PubMed: 17440924]

Kinder SJ, Tsang TE, Quinlan GA, Hadjantonakis A-K, Nagy A, Tam PPL. The orderly allocation of mesodermal cells to the extraembryonic structures and the anteroposterior axis during gastrulation of the mouse embryo. Development 1999;126:4691–4701. [PubMed: 10518487]

Kinder SJ, Tsang TE, Wakamiya M, Sasaki H, Behringer RR, Nagy A, Tam PP. The organizer of the mouse gastrula is composed of a dynamic population of progenitor cells for the axial mesoderm. Development 2001;128:3623–3634. [PubMed: 11566865]

Kispert A, Vainio S, Shen L, Rowitch DH, McMahon AP. Proteoglycans are required for maintenance of Wnt-11 expression in the ureter tips. Development 1996;122:3627–3637. [PubMed: 8951078]

Kulisz A, Simon HG. An evolutionarily conserved nuclear export signal facilitates cytoplasmic localization of the Tbx5 transcription factor. Mol Cell Biol 2008;28:1553–1564. [PubMed: 18160705]

Kwee L, Baldwin HS, Shen HM, Steward CL, Buck C, Buck CA, Labow MA. Defective development of the embryonic and extraembryonic circulatory systems in vascular cell adhesion molecule (VCAM-1) deficient mice. Development 1995;121:489–503. [PubMed: 7539357]

Lawson KA, Meneses J, Pedersen RA. Clonal analysis of epiblast fate during germ layer formation in the mouse embryo. Development 1991;113:891–911. [PubMed: 1821858]

Mossman HW. Comparative morphogenesis of the fetal membranes and accessory uterine structures. Contrib Embryol 1937;26:133–247.

Naiche LA, Harrelson Z, Kelly RG, Papaioannou VE. T-box genes in vertebrate development. Annu Rev Genet 2005;39:219–239. [PubMed: 16285859]

Ozdzenski W. Observations on the origin of primordial germ cells in the mouse. Zoologica Poloniae 1967;17:367–381.

Palmieri SL, Peter W, Hess H, Scholer H. Oct-4 transcription factor is differentially expressed in the mouse embryo during establishment of the first two extraembryonic cell lineages involved in implantation. Dev Biol 1994;166:259–267. [PubMed: 7958450]

Papaioannou VE. T-box genes in development: from hydra to humans. Int Rev Cytol 2001;207:1–70. [PubMed: 11352264]

Pearce JH, Evans MJ. Mml, a mouse Mix-like gene expressed in primitive streak. Mech Dev 1999;87:189–192. [PubMed: 10495285]

Pinson KI, Dunbar L, Samuelson L, Gumucio DL. Targeted disruption of the mouse villin gene does not impair the morphogenesis of microvilli. Dev Dyn 1998;2111:109–121. [PubMed: 9438428]

Rivera-Perez JA, Magnuson T. Primitive streak formation in mice is preceded by localized activation of Brachyury and Wnt3. Dev Biol 2005;288:363–371. [PubMed: 16289026]

Scholer HR. Octamania: the POU factors in murine development. Trends Genet 1991;7:1–5. [PubMed: 2003333]

Scholer HR, Dressler GR, Balling R, Rohdewohld H, Gruss P. Oct-4: a germline-specific transcription factor mapping to the mouse t-complex. EMBO J 1990;9:2185–2195. [PubMed: 2357966]

Schreiner CA, Hoornbeek FK. Developmental aspects of sirenomelia in the mouse. J Morphol 1973;141:345–358. [PubMed: 4753445]

Shalaby F, Rossant J, Yamaguchi TP, Gertsenstein M, Wu X-F, Breitman ML, Schuh AC. Failure of blood-island formation and vasculogenesis in Flk-1 deficient mice. Nature 1995;376:62–66. [PubMed: 7596435]

Snow, MHL. Proliferative centres in embryonic development. In: Johnson, MH., editor. Development in mammals. Amsterdam: North-Holland Publishing Co; 1978.

Sobotta J. Die Entwicklung des Eies der Maus vom ersten Auftreten des Mesoderms an bis zur Ausbildung der Embryonalanlage und dem Auftreten der Allantois. I. Teil: Die Keimblase. Archiv fur mikroskopische Anatomie 1911;78:271–352.

Solloway MJ, Robertson EJ. Early embryonic lethality in Bmp5;Bmp7 double mutant mice suggests functional redundancy within the 60A subgroup. Development 1999;126:1753–1758. [PubMed: 10079236]

Tam, PP.; Beddington, RS. Establishment and organization of germ layers in the gastrulating mouse embryo. In: Chadwick, DJ.; Marsh, J., editors. Postimplanta-tion development in the mouse. Chichester: John Wiley and Sons; 1992. p. 27-41.

Tam PPL, Beddington RSP. The formation of mesodermal tissues in the mouse embryo during gastrulation and early organogenesis. Development 1987;99:109–126. [PubMed: 3652985]

Thomas PQ, Beddington R. Anterior primitive endoderm may be responsible for patterning the anterior neural plate in the mouse embryo. Curr Biol 1996;6:1487–1496. [PubMed: 8939602]

Wilkinson DG, Bhatt S, Herrmann BG. Expression pattern of the mouse T gene and its role in mesoderm formation. Nature 1990;343:657–659. [PubMed: 1689462]

Wilt FH. Erythropoiesis in the chick embryo: the role of endoderm. Science 1965;147:1588–1590. [PubMed: 14260938]

Wolpert, L.; Beddington, R.; Brockes, J.; Jessell, T.; Lawrence, PA.; Meyerowitz, E. Principles of development. Oxford: Oxford University Press; 1998.

Zeigler BM, Sugiyama D, Chen M, Guo Y, Downs KM, Speck NA. The allantois and chorion, which are isolated before circulation or chorio-allantoic fusion, have hematopoietic potential. Development 2006;133:4183–4192. [PubMed: 17038514]

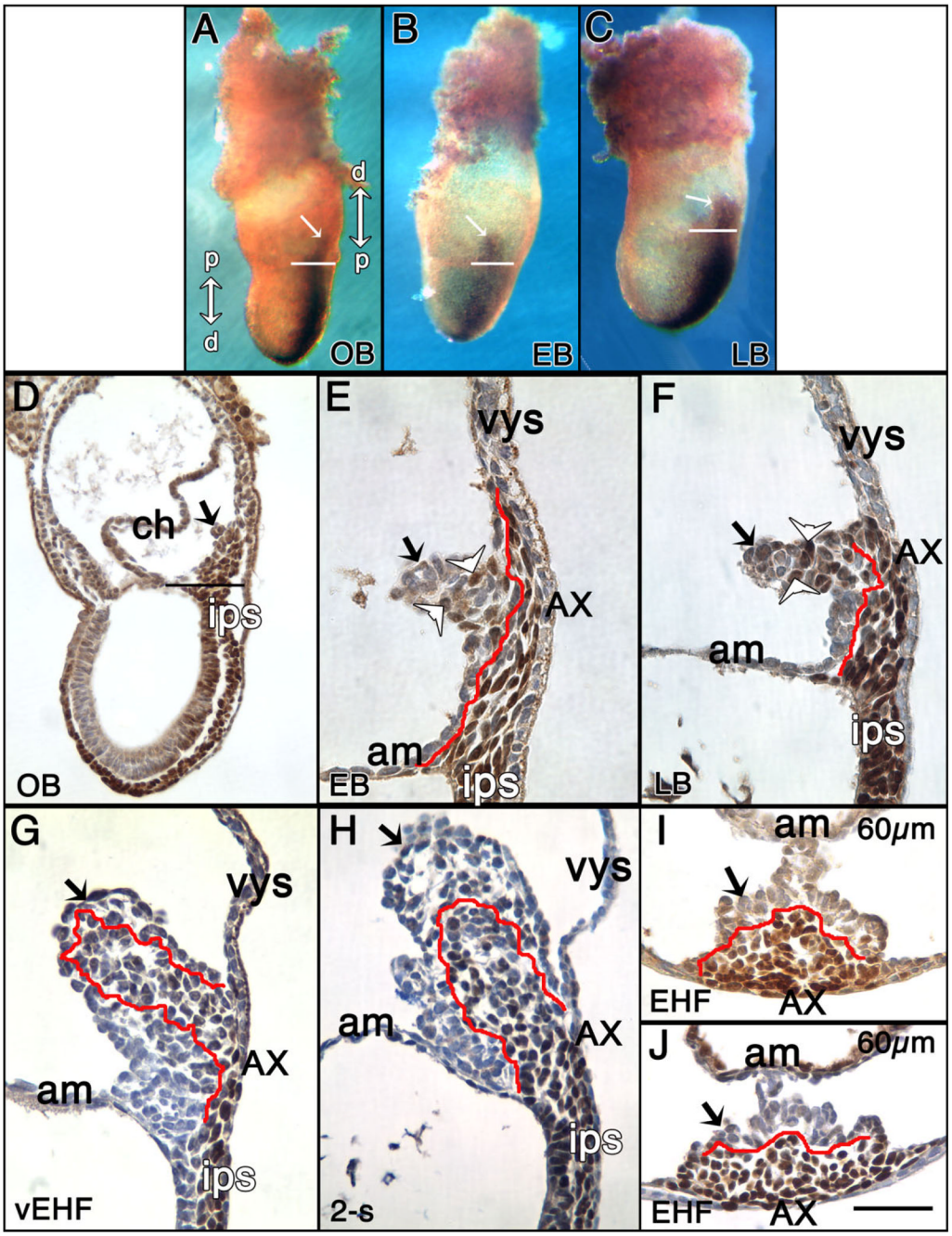

Fig. 1.

Localization of T to the extraembryonic region, allantois and allantois-associated extraembryonic visceral endoderm (AX). Unless indicated, posterior is to the right; anterior is to the left. Double arrows in (A): right: distal/proximal (extraembryonic region), and left: proximal/distal (embryonic region). For the staging key in this and all subsequent figures, refer to the Experimental Procedures. **A–C:** T-immunostained (brown color) whole mount conceptuses. Extraembryonic T (white arrows) is indicated above the amnion (white horizontal bars). A: OB stage. B: EB stage. C: LB stage. D–J: Histological sections prepared after whole mount immunostaining. All sections were briefly counterstained in hematoxylin. Black arrows (all panels) indicate the allantois. **D:** OB stage. Black horizontal bar indicates the embryonic/

extraembryonic junction at the level of the nascent amnion. This is the same embryo as in (A). **E:** EB stage. The red line overlies the extraembryonic extent of the flat polarized T-positive cells that are continuous with the intraembryonic primitive streak (ips) and applied to the overlying allantois-associated extraembryonic visceral endoderm, the AX. The distalmost reach of these cells exceeds the limit of the allantoic bud. White arrowheads in this panel and F indicate round T-positive cells in the distal allantoic bud. **F:** LB stage. The red line is as described in E. At this stage, the distalmost extraembryonic flat polarized T-positive cells are confined to the limit of the allantoic bud. **G:** vEHF stage. The red line outlines the T-positive Allantoic Core Domain (ACD). See text for details. At this stage, the flat polarized T-positive cells adjacent to the AX are less abundant. **H:** 2-s stage. The red line is as in (G). **I,J:** Transverse sections 60 μm above the embryonic/extraembryonic border (see Downs, 2008) through an EHF-stage allantois stained for T (I), and Oct-3/4 (J). The red line outlines the proximal T- and Oct-3/4-domains, which are symmetric about the A–P axis, but biased toward the ventral AX. am, amnion; ch, chorion; ips, intraembryonic posterior primitive streak; vys, visceral yolk sac. Scale bar in J = 366 μm in A–C, 100 μm in D, 50 μm in G–J, 33.3 μm in E,F.

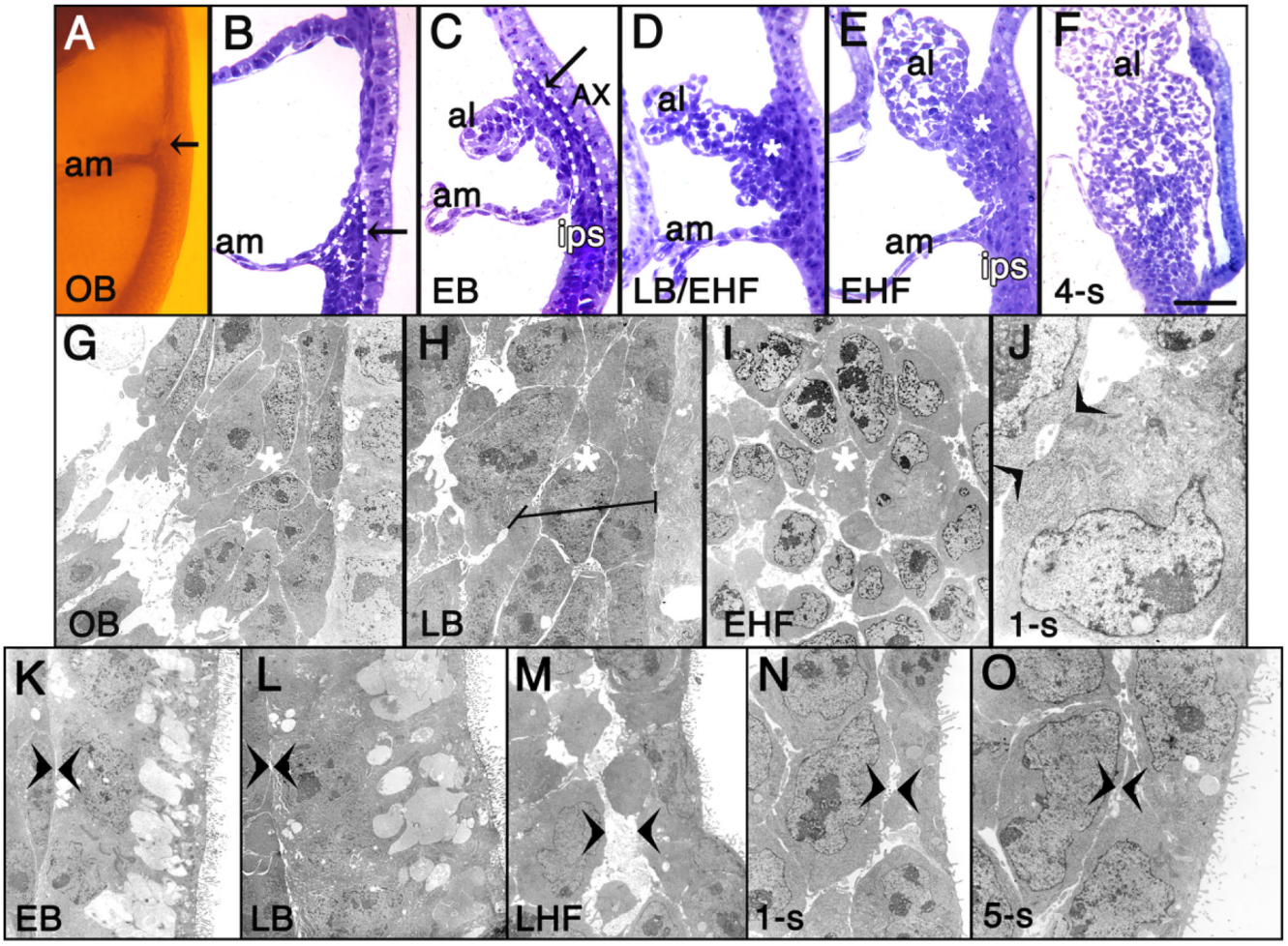

Fig. 2.

The primitive streak extends into the exocoelom. **A:** OB stage, posterior half egg cylinder, Araldite plastic. Extraembryonic primitive streak (arrow) above amnion (am). B–F: Azure B-stained plastic sections. **B:** OB stage (from A). The primitive streak's posterior end forms a wedge of cells (outlined in white hashed line) extending into the exocoelom. **C:** EB stage. Extraembryonic streak cells (outlined in white hashed line, and highlighted by black arrow) are polarized and closely applied to the overlying highly vacuolated AX. **D:** LB/EHF stage. Expanded extraembryonic streak, designated "ACD" (Allantoic Core Domain; asterisk in this and E,F). **E:** EHF stage. **F:** 4-s stage. G–O: TEM images. **G:** OB stage (from A,B). Darkly stained extraembryonic streak cells, left (surrounding asterisk in this and panels H,I), adjacent to less electron dense AX cells, right (visible only in G,H). **H:** LB stage. Horizontal line: elongated streak cells, left of basal surface of less electron dense AX cells, right. **I:** EHF stage. Cells within ACD (asterisk) display loosened contacts. **J:** 1-s stage. Single ACD cell with large Golgi zone, polyribosomes, and simple adhesion junctions to adjacent cell (arrowheads). **K–O:** TEMs, AX association with allantois. Arrowheads: contact point between AX, allantois. EB, LB, LHF, 1-s, and 5-s stages, respectively. Abbreviations as in Figure 1; al, allantois. Scale bar in F = 50 μm in B–E, 100 μm in A,F, 9 μm in G, 4.2 μm in H, 5.5 μm in I, 1.6 μm in J, 7.5 μm in K, 6.2 μm in L, 5.6 μm in M, 6.2 μm in N, 4.9 μm in O.

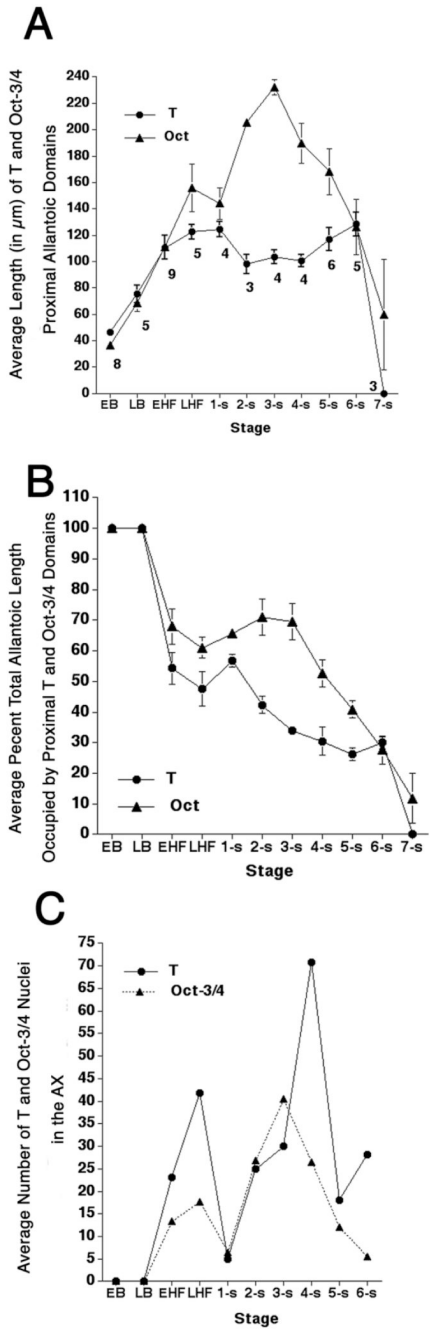

Fig. 3.

T- and Oct-3/4 allantoic domains and numbers of positive nuclei in the allantois-associated extraembryonic visceral endoderm (AX). **A:** Average length of proximal T- and Oct-3/4 (Downs, 2008) domains according to developmental stage. Specimen numbers are for T-immunostained specimens in all panels. Those for Oct-3/4 were previously reported (Downs, 2008). **B:** Percent of the total allantoic length occupied by the proximal T and Oct-3/4 (Downs, 2008), domains, according to developmental stage. **C:** Average numbers of AX cells containing nuclear T and Oct-3/4 (Downs, 2008), according to developmental stage. Note that the AX does not contain T- and Oct-3/4-positive nuclei until the early headfold (EHF) stage. Error bars

in A, B are the standard error of the mean (SEM). The SEM is not indicated in (C) because the range in the number of nuclei at each developmental stage was very wide.

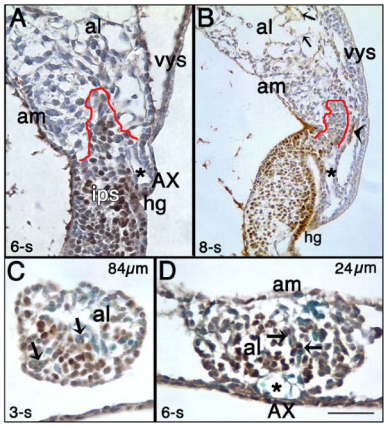

Fig. 4.

The allantoic T-domain at later somite stages and colocalization with Flk-1. T-immunostained (brown color) histological sections counterstained with hematoxylin (purple color). **A:** 6-s stage, sagittal section. Part of the T-domain is outlined in red. The length of this domain has not changed from previous stages (see Fig. 3), but its girth appears to be reduced (see text). The asterisk indicates the “vessel of confluence” (VOC), which is the site of amalgamation between the arterial vessels of the allantois, yolk sac and embryo (Downs et al., 1998). **B:** 8-s stage, sagittal section. By this stage, the condensed core of the allantois, outlined in red, is still present, but T is no longer robustly expressed there. The asterisk indicates the VOC, and the arrowhead indicates a patch of mesothelium where T is expressed in its cytoplasm. Small arrows indicate T-positive presumptive endothelial cells. **C:** 3-s stage, transverse section through the allantois, 84 μm from its boundary with the intraembryonic primitive streak (IPS). T colocalizes with many Flk-1–positive cells (royal blue color; arrow indicates co-stained cells). **D:** 6-s stage, transverse section through the allantois 24 μm from its boundary with the IPS. Arrows indicate T/Flk-1 co-stained cells. Asterisk indicates the VOC. hg, hindgut. Other abbreviations as in the previous figures. Scale bar in D = 100 μm in A,B, 50 μm in C,D.

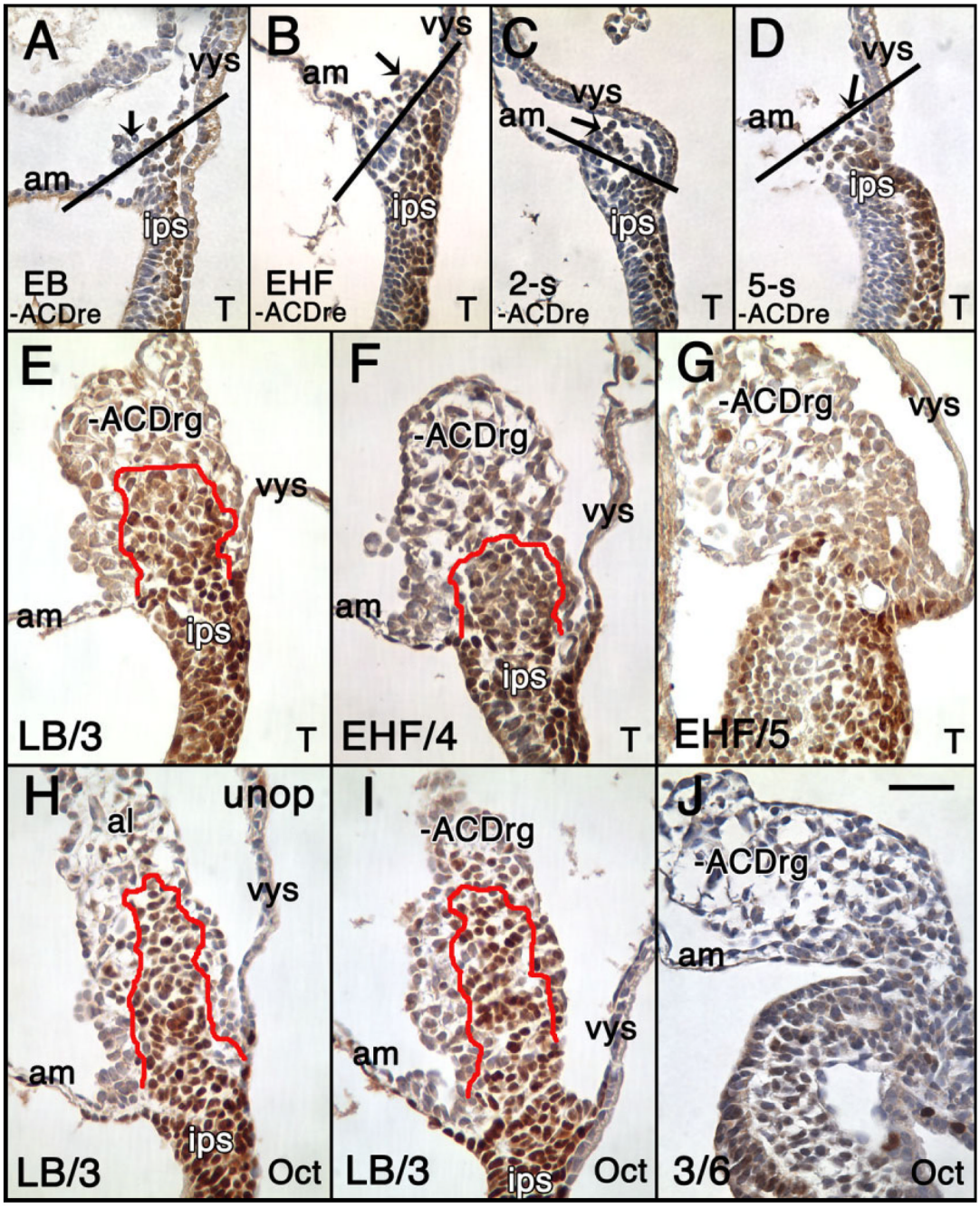

Fig. 5.

Status of the Allantoic Core Domain (ACD) in −ACD regenerates is revealed by T-and Oct-3/4 immunostaining. A–D: Immediately fixed and T-immunostained (brown color) sagittal sections through the posterior end of the conceptus after removing the allantois (−ACDre). Arrows indicate what remains of the allantois. The black line indicates the site of insertion of the allantois with the adjacent amnion and yolk sac, as previously defined (Downs and Harmann, 1997). **A:** EB stage. **B:** EHF stage. **C:** 2-s stage. **D:** 5-s stage. E–J: T- (E–G) and Oct-3/4 (H–J) immunostaining (brown color) −ACDrg (E–G,I,J), or unoperated (H) allantois sagittal profiles, after appropriate time in culture. Stages in the lower left indicate the initial stage/final stage after culture. The red line outlines the ACD. **E:** LB/3-s stage, −ACDrg contains

the ACD. **F,G:** EHF/4 and EHF/5 stages showing ACD (F) and its absence (G). H–J: Oct-3/4-stained (brown color) sagittal profiles of unoperated control allantois (al) (H) and allantoic regenerates (−ACDrg). **H:** LB/3-s stage, unoperated allantois with ACD. **I:** LB/3 stage, −ACDrg contains the ACD. **J:** 3/6-s stage, −ACDrg lacks the ACD. Scale bar in J = 50 μm in A–J.

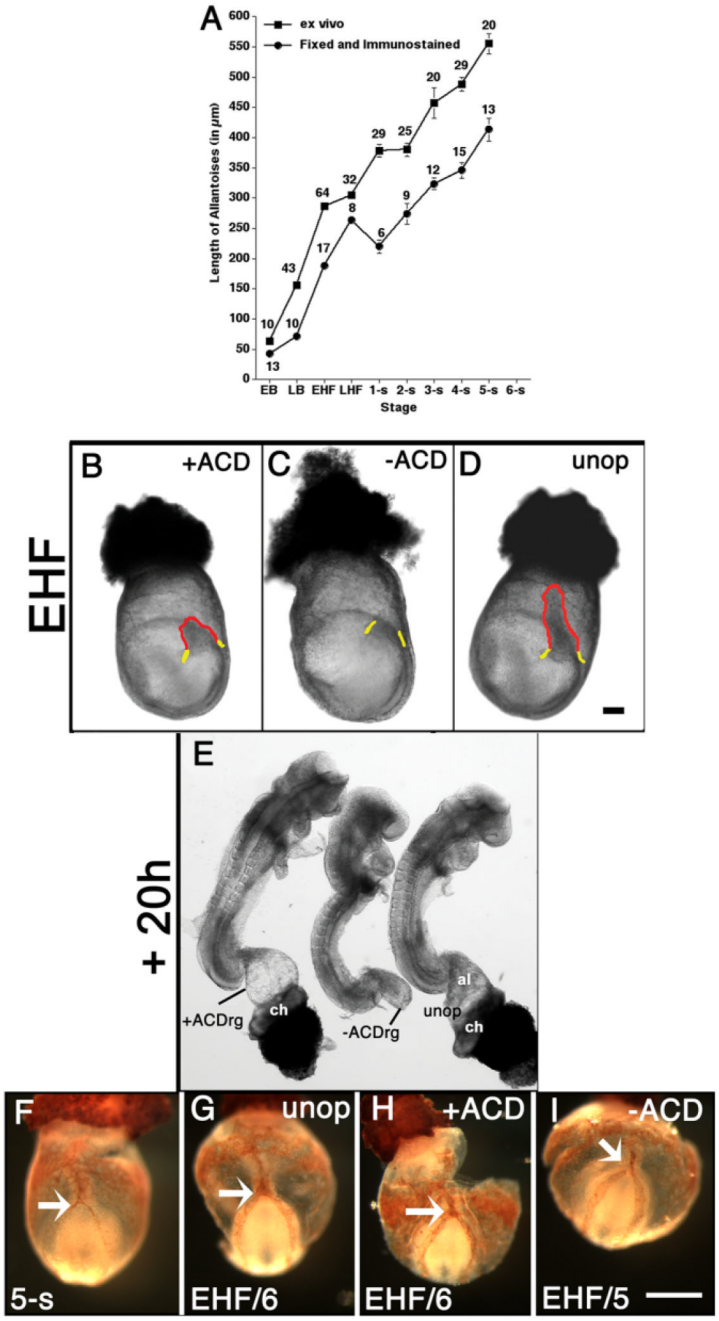

Fig. 6.

The Allantoic Core Domain (ACD) is essential for allantoic elongation but not vascularization. **A:** Average length of allantoises: freshly dissected (squares); fixed and immunostained for T (this study) and Oct-3/4 (previous study) (circles). Approximate mean shrinkage factor for all stages, 1.6 (see the Experimental Procedures section). B–D: Whole conceptuses, EHF stage. **B:** ~133 µm proximal allantois (red outline, "+ACD") remains after removal of the distal allantoic region. **C:** The intraembryonic primitive streak (IPS) site (yellow) above which the entire whole allantois was removed ("−ACD"). **D:** Unoperated allantois (red outline). **E:** Stage-matched embryos from (B–D) after 20 hr culture. F–I: Mec 13.3 Platelet Cell Adhesion Molecule-1 (PECAM-1)-stained (seethe Experimental Procedures section) whole conceptuses

(posterior end is up), freshly dissected (F), 10 hr culture, 50% fetal calf serum (see the Experimental Procedures section). G,I: For cultured embryos, initial stage/final stage in lower left of each panel. White arrows indicate the point of connection at the vessel of confluence (VOC) between the patterned allantoic vasculature and the embryonic dorsal aortae. **F:** 5-s stage, freshly dissected conceptus. **G:** Cultured EHF/6-s stage, unoperated conceptus. **H:** Cultured EHF/6-s stage, +ACD conceptus. **I:** Cultured EHF/5-s stage, −ACD conceptus. This conceptus shows lack of fusion between the left embryonic dorsal aorta and the allantoic vasculature (see text for details). Scale bars = 100 μm in D (applies to B–E), 100 μm in I (applies to F–I).

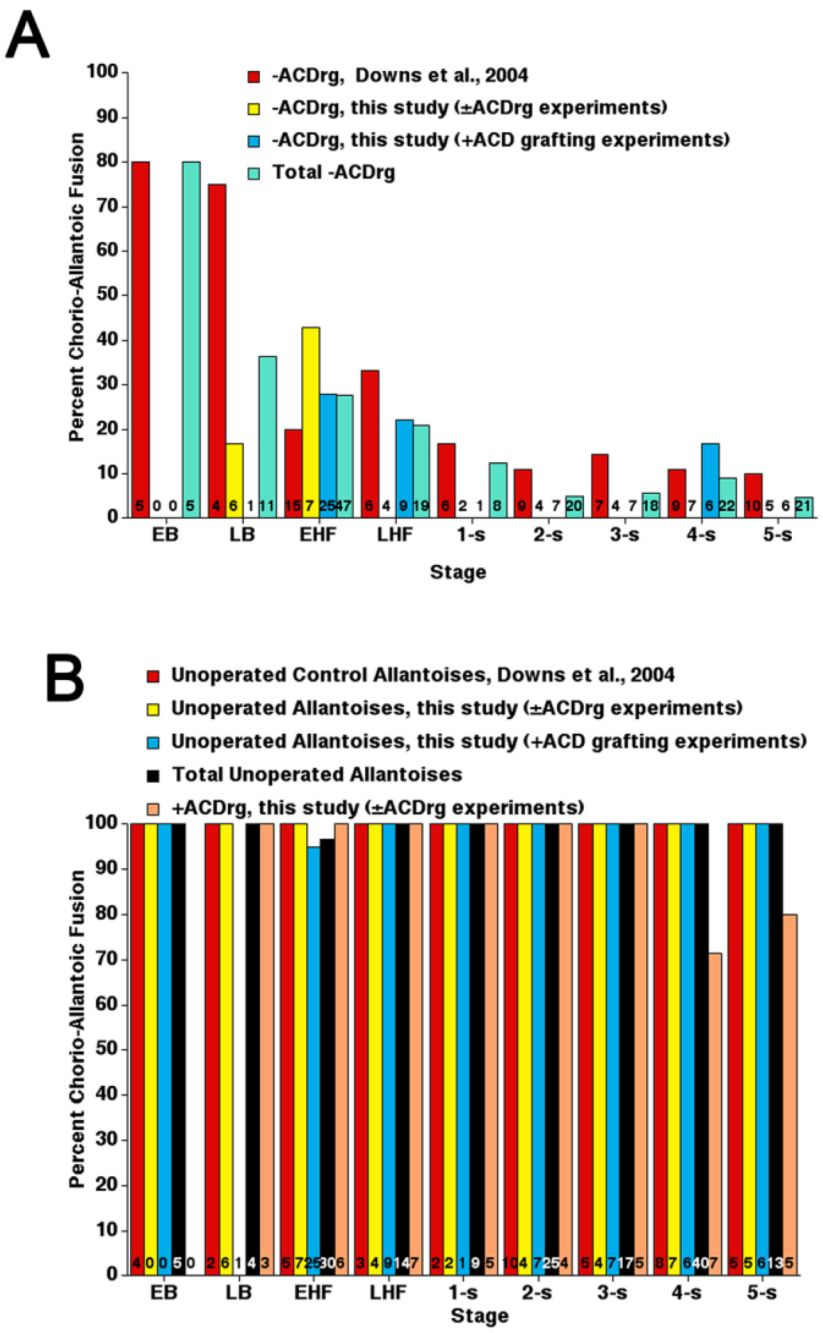

Fig. 7.

Frequency of chorio-allantoic union in −ACD regenerates, +ACD regenerates, and unoperated allantoises, 20 hr in culture. Data from different studies are reported separately to illustrate similar outcomes. **A:** −ACD regenerates. **B:** Unoperated allantoises and +ACD regenerates, the latter of which have not previously been investigated. Numbers of specimens examined are indicated at the base of each bar. ACD, Allantoic Core Domain.

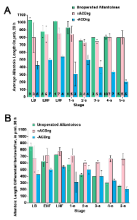

Fig. 8.

Average lengths and length differentials in allantoic regenerates, 20 hr in culture. Data are from the current study to provide direct comparisons between each class of allantoic manipulation. **A:** Comparison of average final lengths after 20 hr in culture between two classes of allantoic regenerates, −ACDrg and +ACDrg, and unoperated control allantoises. Numbers of specimens examined are indicated at the base of each bar and apply to both panels (A,B). **B:** Comparison of average length differentials, i.e., the length achieved by unoperated, −ACDrg, and +ACDrg in culture. These lengths were calculated by subtracting the length of the allantois at the start of culture from its final length at the end of culture, indicated on the y-axis as “before/after” (see the Experimental Procedures section).

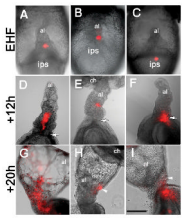

Fig. 9.

Fate mapping reveals distinct contributions to the allantois. A–C: EHF stage. 1,1′, di-octadecyl-3,3,3′,3′,-tetramethylindo-carbocyanine perchlorate (DiI, orange color) was applied to conceptuses (posterior end is up). **A:** Central Allantoic Core Domain (ACD). **B:** Right flank proximal allantoic region. **C:** Midline intraembryonic primitive streak (IPS). **D–F:** Labeled descendants, 12 hr, specimens in (A–C). White arrows: allantois/IPS boundary. **G–I:** Labeled descendants, applications similar to (A–C), 20 hr culture. White arrowheads, allantoic flank. Abbreviations as in the previous figures. Scale bar in I = 500 μm in A–I.

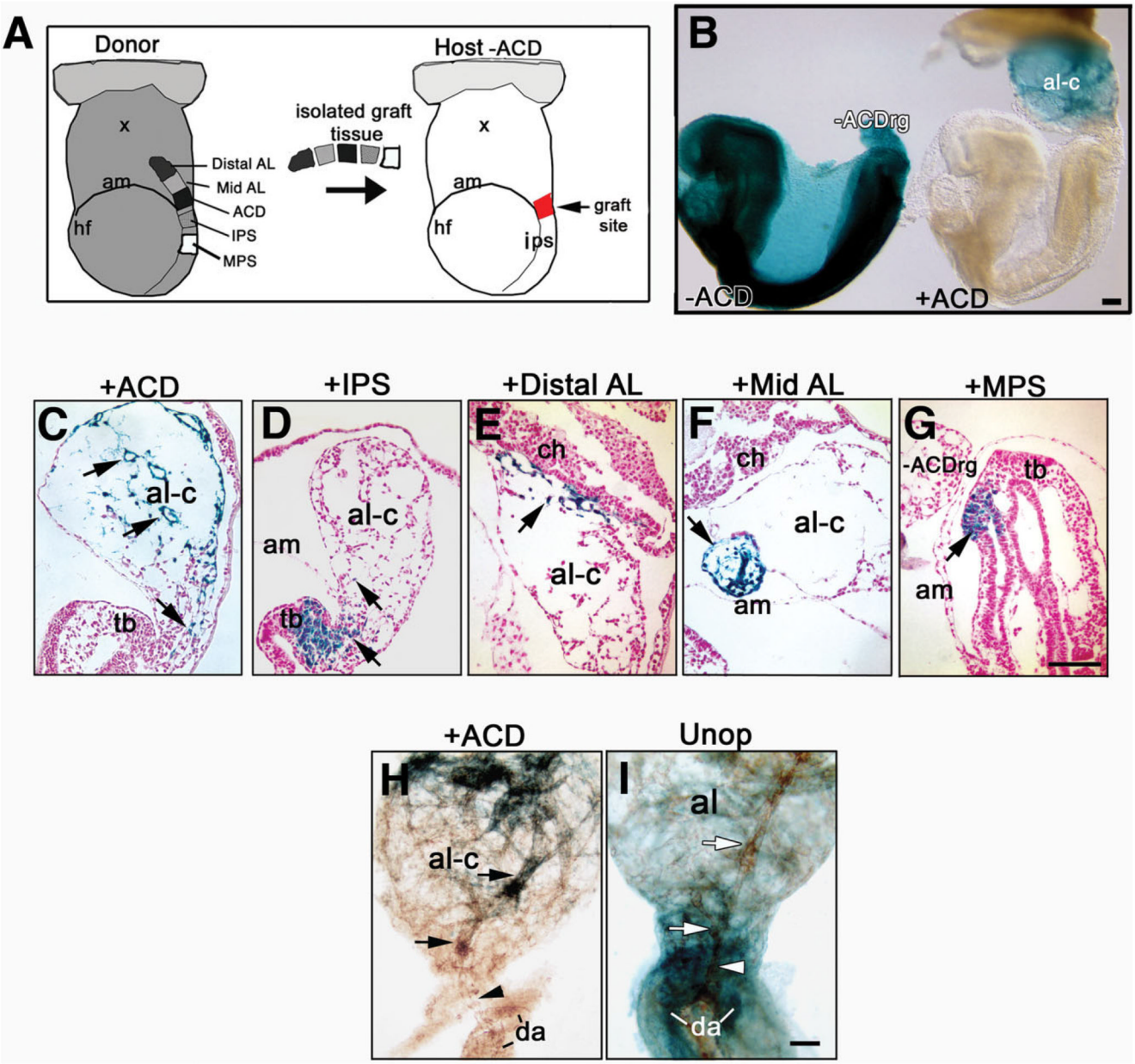

Fig. 10.

Grafting the proximal allantois and nearby regions. **A:** Schematic diagram: Left: Donor *ROSA 26/+* conceptus showing tissue taken for grafts: distal, mid-allantoic thirds (Distal, Mid-AL), Allantoic Core Domain (ACD), intraembryonic posterior (IPS), mid-(MPS) primitive streak; Right: Host −ACD after removal of the host allantois. The arrow indicates the site (red square) into which the tissue pieces in A were grafted. **B:** Left conceptus: X-gal whole-mount stained donor conceptus after allantoic removal (−ACD), 20 hr culture (left), shows nonelongated −ACDrg; Right conceptus: host conceptus cultured in parallel after grafting with ACD (+ACD) shows elongated and fused chimeric allantois (al-c). C–G: Histological sections, X-gal–positive (blue) donor (arrows in all panels). **C:** +ACD graft contributes to proximal midline (lower arrow) and distal region (two upper arrows) of the chimeric allantois. **D:** IPS contribution to embryonic tail bud (tb) and limited contribution to the chimeric allantoic

regenerate. **E:** Distal AL contribution to the distal region of the chimeric allantoic regenerate. **F:** Mid AL graft contributes to mid-allantoic region, not well incorporated, of the chimeric allantoic regenerate. **G:** mid-primitive streak (MPS) graft contributes to tail bud only. The -ACDrg does not contain grafted cells. H,I: Whole mount Platelet Endothelial Cell Adhesion Molecule-1 (PECAM-1) -immunostained (brown color) allantoises, 20 hr culture from headfold (HF) stages. Compared with the robust Mec 13.3 immunostain in Figure 6F–I, immunostaining here was with Armenian hamster anti-mouse PECAM-1, which produced a less robust signal (see the Experimental Procedures section). **H:** Chimeric allantoic regenerate containing +ACD graft (blue cells); point of connection (black arrowhead) between central allantoic vessel (black arrows), fused portion of paired fetal dorsal aorta (da) slightly separated. **I:** Unoperated donor conceptus exhibits central vessel (white arrows) appropriately aligned and connected to (white arrowhead) dorsal aorta. Scale bars = 100 μm in B, 100 μm in G (applies to C–G), 100 μm in I (applies to H,I).

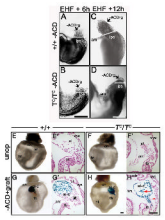

Fig. 11.

The Allantoic Core Domain (ACD) rescues elongation in T^C/T^C mutant allantoises. A–D: Posterior views of whole embryos to demonstrate the extent of allantoic regeneration after removing the entire allantois at the EHF stage. The white bar in all four panels indicates the boundary between the allantois and the intraembryonic primitive streak (IPS). **A,C:** +/+, −ACDrg after 6 hr (A) and, after 12 hr (C) of culture. **B,D:** T^C/T^C −ACDrg after 6 hr (B) and, after 12 hr (D) of culture. Note that between 6 and 12 hr, the T^C/T^C regenerate did not further elongate. See text for details. **E,F:** Whole-mount (E,F) and histological sagittal sectional views (E',F') of +/+ and T^C/T^C, reveal short T^C/T^C allantois. Allantoic areas (see the Experimental Procedures section): +/+: 0.15 ± 0.03 mm^2 (n = 3); T^C/T^C : 0.03 ± 0.01 mm^2 (n = 2). **G,H:** Whole-mount (G,H) and sagittal sectional views (G′,H′) of +ACD grafts into +/+ and T^C/T^C −ACD hosts (G) +/+ regenerate, area: 0.11 ± 0.02 mm^2, n = 3; (H) T^C/T^C allantoic chimera, vascularization (red arrow) and predominantly donor ACD-derived cells, proximal mutant T^C/T^C host-derived cells (red arrowhead) flank remnant's proximal core, area = 0.09 ± 0.02 mm^2 (n = 2). Abbreviations as in previous figures. Other abbreviations: hf, head-fold; ht, heart. Scale bars = 500 μm in B (applies to A,B); 500 μm in D (applies to C,D); 500 μm in H (applies to E–H, and 100 μm in H′ (applies to E′–H′).

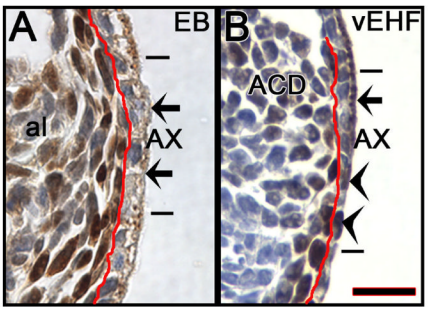

Fig. 12.

Cytoplasmic and nuclear T within the allantois-associated extraembryonic visceral endoderm (AX). Enlarged sagittal views of the AX immunostained with T (brown color), taken from Figure 1. Both panels were counter-stained with hematoxylin; as a result, those cells that do not contain nuclear T exhibit purple nuclei. **A:** EB stage. From Figure 1E. The red line separates the AX, right, from the polarized cells of the closely applied extraembryonic component of the primitive streak (XPS). Short horizontal bars indicate the extent of the AX, between which the arrows points to examples of cytoplasmic T within the apical vesicles. Note the uniform thickness of the AX. The nuclei in these cells are purple, showing absence of T there. **B:** vEHF stage. From Figure 1G. All indicators are the same as in A, with the exception of the arrowheads, which indicate examples of T-positive nuclei (black/brown color) within the proximal region of the AX. Note the gradation in thickness of the AX, from proximal-to-distal (bottom-to-top). Scale bar in B = 16.7 μm in A,B.

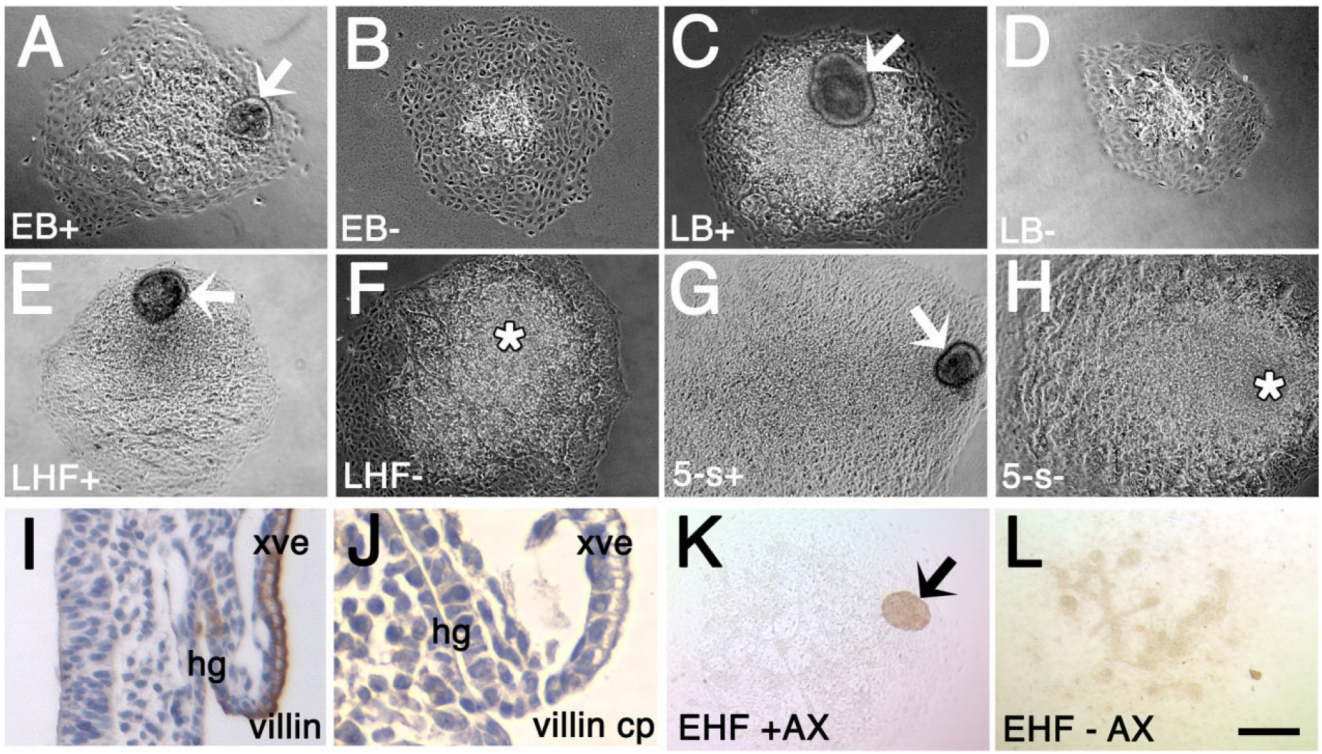

Fig. 13.

The Allantoic Core Domain (ACD) is established in collaboration with allantois-associated extraembryonic visceral endoderm (AX). **A**–**H:** 20-hr allantoic explants with (+; A,C,E,G) or without (−; B,D,F,H) AX. **I,J:** Villin-stained (I, brown) freshly dissected 8-s conceptus (J). Pre-binding villin antibody with control peptide shows villin specificity. K,L: EHF, villin-stained. **K:** +AX. **L:** −AX. Villin does not stain the allantois. xve, extraembryonic visceral endoderm. Other abbreviations as in the previous figures. Scale bar in L = 200 μm in A–H,K,L, 95 μm in I, 19 μm in J.

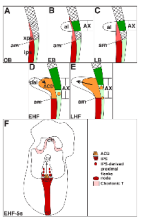

Fig. 14.

The allantois is built by extraembryonic and intraembryonic components of the posterior primitive streak. A–E: Schematic sagittal views; (F) Posterior "frontal" view. **A:** Extension of the posterior primitive streak into the extraembryonic region. xps, extraembryoic primitive streak (pink); ips, intraembryonic primitive streak (red); am, amnion. The hatched area overlying the xps indicates the visceral endoderm that contains cytoplasmic T. The light green area beneath it is the squamous embryonic visceral endoderm. **B:** EB stage. The allantoic bud (al) has emerged from the distal portion of the pink xps which, at this time, exceeds the limit of the allantois. The bright green area overlying the allantoic bud is the allantois-associated extraembryonic visceral endoderm (AX), which at this time contains cytoplasmic T. **C:** LB stage. The xps is thicker than at the previous stage, and the allantoic bud has elongated. The AX still contains cytoplasmic T. **D:** EHF stage. The xps has become transformed into the Allantoic Core Domain (ACD; orange), possibly by influence of the AX at the previous bud stages. The allantois is now continuous with the ips (red). T-positive nuclei (small round orange circle) have begun to appear in the proximal portion of the AX, which is becoming more squamous and similar to the embryonic visceral endoderm (light green). The more distal cytoplasmic T-containing portion of the AX (bright green) appears to have shifted distally toward the chorion. Information within the distal region of the allantois (dal) may be feeding back onto the ACD to regulate allantoic elongation. **E:** LHF stage. The ACD (orange) is now fully mature, and is driving allantoic elongation toward the chorion (thick straight arrow). T-positive nuclei continue to be found in the AX, whose cytoplasmic T-containing region appears to continue its upward shift. **F:** Summary of the relationship of the embryonic antero–posterior axis (red) (posterior end is up), with its anterior node (hatched red oval) and intraembryonic posterior primitive streak (ips, hatched red inverted trapezoid) to the ACD (hatched orange trapezoid). By the HF stages, the ACD produces a midline file of cells (vertical arrow) in direct alignment with the embryonic antero–posterior axis, the primitive streak (red color). In the distal region, this midline file branches out (scattered small arrows) and fills the distal portion of the allantois. The IPS contributes cells to the proximal allantoic flanks (red circles). The chorionic ectoderm (ch) is T-positive (light pink color; Inman and Downs, 2006a), though T's function in this tissue is not yet known.

TABLE 1

Location of Labeled Descendants After Application of DiI (20 hr in Culture)[a]

DiI application into the central ACD (6–133 μm of the ACD's boundary with the intraembryonic IPS)[b] N = 40						
	EB[c]	**LB[d]**	**EHF**	**LHF**	**1–2-s**	**3–5-s**
Central allantoic file	0/4 (0)	2/6 (33.3%)	10/10 (100%)	4/4 (100%)	3/3 (100%)	3/3 (100%)
DiI application into the left or right flanks of the ACD[e](6–133 μm of the ACD's boundary with the intraembryonic IPS)N = 24						
Allantoic flanks	ND	ND	10/10 (100%)	2/2 (100%)	7/7 (100%)	5/5 (100%)
DiI application into the central region of intraembryonic IPS (6–133 μm from the streak's boundary with the allantois)N = 40						
Tail bud region	1 (33.3%)	1 (16.7%)	10 (58.8%)	4 (80.0%)	1 (25.0%)	3 (60.0%)
Proximal allantois	1 (33.3%)	0	3 (17.6%)	0	0	0
Tail bud/proximal allantois	1 (33.3%)	5 (83.3%)	4 (23.5%)	1 (20.0%)	3 (75.0%)	2 (40.0%)

[a] DiI, 1,1′, di-octadecyl-3,3,3′,3′,-tetramethylindo-carbocyanine perchlorate; ACD, Allantoic Core Domain; IPS, intraembryonic primitive streak; EB, early bud stage; LB, late bud stage; EHF, early headfold; LHF, late headfold; ND, not determined.

[b] The 43 total injections were applied to the central ACD (EHF stage) of which 3/43 were >133 μm; these descendants localized to a band at the chorio-allantoic fusion junction.

[c] In 4/4 specimens, labeled descendants were concentrated in the distal region.

[d] In 4/6 specimens, labeled descendants were found throughout the allantois.

[e] All descendants remained within the same plane of dye application. Final distribution of labeled cells: 7/24 (29.2%) proximal flank; 11/24 (45.8%) mid-region; 5/24 (20.8%) distal-third. There was no obvious preference for final location with regard to stage.

TABLE 2

Transplantations of Donor Tissue Into the Embryonic/Extraembryonic Junction of −ACD Host Conceptuses (≥EHF Stages)[a]

Donor → Host (stage, expts)	Total no. grafts % unincorp.	A	B	C	D	E
ACD→+/+ (HF, N = 9)	21 14.3%	0	2/18 (11.1%)	0	16/18 (88.9%)	50.0% 649.3 ± 24.8; N = 17
Unoperated (HF)						100% (N = 18) 731.1 ± 29.1; N = 13
−ACD (HF)						23.1% (N = 23) 433.9 ± 17.5; N = 18
ACD→+/+ (1–4-s, N = 2)	7 0%	0	0	0	7/7 (100%)	28.6 528.0 ± 76.2; N = 6
Unoperated (1–4-s)						100% (N = 22) 763.3 ± 21.2; N = 9
−ACD (1–4-s)						0% (N = 12) 406.2 ± 39.7 (N = 11)
IPS→ +/+ (HF, N = 5)	12 8.3%	5/11 (45.4%)	1/11 (9.1%)	5/11 (45.4%)	0	18.1% 400.3 ± 47.1; N = 4
MPS→ +/+ (HF, N = 2)	7 28.6%	5/5 (100%)	0	0	0	0
Mid-AL→+/+ (HF, N = 3)	6 33.3%	0	4/4 (100.0%)	0	0	0 311.3 ± 58.8; N = 3
Distal AL→+/+ (HF, N = 3)	10 50.0%	0	5/5[b] (100%)	0	0	40.0% 480.2 ± 25.0; N = 5
ACD→ +/+[c] (HF, N = 4)	3 0%	0	0	0	3/3 (100%)	67.0% 577.8 ± 80.1; N = 3
ACD → T^C/T^C (HF)	2 0%	0	0	0	2/2 (100%)	0 483.4 ± 16.67; N = 2

[a] A: restricted to host posterior region. B: restricted locally in host allantois. C: incorporated into host posterior region and base of the allantois. D: spanning the length of the allantois. E: Percentage of allantoic remnants that have fused with the chorion. All specimens were scored for fusion (N = number of specimens examined for fusion). Average allantoic length in μm ± SEM; number of specimens measured (not all specimens were measured at the end of the culture period). Only the lengths of chimeric allantoises (i.e., those that contained grafted cells) are included in the length measurements.

[b] In one exceptional graft, cells from the donor distal third created a slender file of cells along the length of the allantois, culminating in a congregation of donor cells in the distal allantoic third.

[c] The gray shading indicates cohorts in the same T experiment.

TABLE 3

Allantois/AX Associations After 20- to 24-hr Culture and Allantoic Explant Diameters (in μm)[a]

	+AX		−AX	
Stage	No. AX attached/total (%)	Explant diameter ± SEM (N)	Explant diameter ± SEM (N)	*P* value
EB	4/4 (100.0%)	636.4 ± 63.9 (4)	465.3 ± 105.1 (3)	0.20
LB	10/11 (90.9%)	792.0 ± 54.9 (10)	636.6 ± 40.2 (9)	0.04
EHF	9/13 (69.2%)	974.5 ± 105.3 (9)	867.3 ± 63.1 (13)	0.36
LHF	4/4 (100.0%)	1027.7 ± 112.0 (4)	1076.0 ± 100.1 (4)	0.72
1-s	4/4 (100.0%)	950.6 ± 49.4 (4)	950.0 ± 91.1 (4)	1.0
2-s	2/5 (40.0%)	1380.0 ± 30.0 (2)	1108.4 ± 191.6 (2)	0.31
3-s	4/5 (80.0%)	1378.0 ± 186.0 (4)	1385.0 ± 71.8 (4)	0.98
4-s	3/5 (75.0%)	1493.3 ± 53.3 (3)	1220.8 ± 179.1 (2)	0.17
5-s	5/5 (100.0%)	1265.7 ± 92.3 (5)	1325.0 ± 68.4 (4)	0.65

[a]Numbers of explants reflect the sum total of explants, all of which survived culture. In those cases where the AX was no longer associated with the allantois, it was found floating in the medium. Such explants were excluded from the diameter measurements.